Wannier functions of isolated bands in one-dimensional crystals

A. Bruno-Alfonso[*] and D. R. Nacbar

Departamento de Matemática, Faculdade de Ciências, UNESP—Universidade Estadual Paulista,
Avenida Luiz Edmundo Carrijo Coube 14-01, 17033-360 Bauru-SP, Brazil

We present a simple procedure to obtain the maximally localized Wannier function of isolated bands in one-dimensional crystals with or without inversion symmetry. First, we discuss the generality of dealing with real Wannier functions. Next, we use a transfer-matrix technique to obtain nonoptimal Bloch functions which are analytic in the wave number. This produces two classes of real Wannier functions. Then, the minimization of the variance of the Wannier functions is performed, by using the antiderivative of the Berry connection. In the case of centrosymmetric crystals, this procedure leads to the Wannier-Kohn functions. The asymptotic behavior of the Wannier functions is also analyzed. The maximally localized Wannier functions show the expected exponential and power-law decays. Instead, nonoptimal Wannier functions may show reduced exponential and anisotropic power-law decays. The theory is illustrated with numerical calculations of Wannier functions for conduction electrons in semiconductor superlattices.

I. INTRODUCTION

The Wannier functions (WFs) form an appropriate basis to express localized states in crystalline solids. In his seminal paper of 1959, Kohn reported the basic theory to obtain exponentially localized WFs for one-dimensional (1D) crystals with inversion symmetry.[1] This kind of WF has been called a Wannier-Kohn function.[2] Recently, the calculation of the Wannier-Kohn functions of isolated bands has been addressed.[3] The phase of Bloch functions (BFs) was chosen according to the symmetry class of the band and the WF was calculated by numerical integration of the BFs. Moreover, the theory was applied to study conduction states in semiconductor superlattices.[3,4] He and Vanderbilt[5] have analyzed the asymptotic behavior of the Wannier-Kohn functions. These authors found a power-law decay besides the exponential behavior predicted by Kohn[1] and claimed their results are valid for noncentrosymmetric 1D crystals.[5]

Eilenberger extended the Kohn's theory to deal with WFs in 1D crystals without inversion symmetry.[6] However, important aspects of the problem remain unsolved. Marzari and Vanderbilt[7] have established a general procedure to obtain the maximally localized Wannier functions (MLWFs). Their procedure has been successfully applied to three-dimensional crystals and deals with isolated, as well as composite, bands. However, they perform the minimization of the total spread of the WFs numerically. Smirnov and Usvyat[8] have reported a variational method, while Bhattacharjee and Waghmare[9] have presented an expression based on parallel transport. Moreover, Prodan has studied the Bloch functions for linear molecular chains[10] and has called the attention to the existence of WFs with reduced exponential decay in strictly 1D crystals.

This work has three main motivations: (i) the need for a simple procedure to obtain the maximally localized Wannier function of an isolated band in 1D crystals without inversion symmetry, (ii) the question on whether a real Wannier function presents the maximal localization, and (iii) a deeper understanding of the asymptotic behavior of the Wannier functions in 1D crystals.

In Sec. II we present fundamental concepts on Wannier functions of simple bands. Their localization is measured by the variance of the corresponding probability distribution. Moreover, we give the phase shift one should perform on the Bloch functions in order to obtain the MLWF. Furthermore, we explain why we may limit ourselves to deal with real WFs. It should be noticed, however, that an initial guess for the Bloch functions is needed. In Sec. III, the BFs are obtained by a transfer-matrix technique. There, the Bloch condition is applied to an initial position x_0, which plays a singular role throughout this paper. In Sec. IV, the phase of the BFs is fixed in analogy with the theory of Kohn.[1,3] This first stage gives two classes of WF. The second stage, which gives the MLWF, is explained in Sec. V. There we also discuss whether the MLWF depends on x_0.

In Sec. VI, we approach the asymptotic behavior of the Wannier functions. There, we analyze the exponential and the power-law decays and obtain interesting results. Moreover, the particular case of centrosymmetric crystals is analyzed in Sec. VII. The theory is illustrated in Sec. VIII, where numerical calculations of Wannier functions for conduction electrons in semiconductor superlattices are presented. Furthermore, in Sec. IX, we emphasize our main results. The appendixes at the end of the paper contain further details of the theory.

II. WANNIER FUNCTIONS

For a 1D crystal with lattice period a along the x axis, the Bloch functions (BFs) satisfy

$$\psi_{j,k}(x + a) = e^{ika}\psi_{j,k}(x), \tag{1}$$

where j is the band index and k is the wave number. Moreover, the BFs are usually chosen as periodic functions of k, namely

$$\psi_{j,k+2\pi/a}(x) = \psi_{j,k}(x). \tag{2}$$

Hence, each Bloch state may be expressed by a Fourier series, i.e.,

$$\psi_{j,k}(x) = \sum_n w_{j,n}(x)\exp(ikna), \tag{3}$$

with $w_{j,n}(x) = w_j(x-na)$ and

$$w_j(x) = \frac{a}{2\pi}\int_{-\pi/a}^{\pi/a}\psi_{j,k}(x)dk. \tag{4}$$

The Fourier coefficient $w_{j,n}(x)$ is the Wannier function of the jth band and the nth cell. We normalize the BFs to unity over an elementary unit cell. Therefore, we get

$$\int_{-\infty}^{\infty}\psi_{j,k}^*(x)\psi_{j',k'}(x)dx = \frac{2\pi}{a}\delta_{j,j'}\delta(k'-k) \tag{5}$$

for k and k' in the first Brillouin zone, and

$$\int_{-\infty}^{\infty}w_{j,n}^*(x)w_{j',n'}(x)dx = \delta_{j,j'}\delta_{n,n'}. \tag{6}$$

We note that $\psi_{j,k}(x)$ satisfies the Bloch condition in Eq. (1) and the time-independent Schrödinger equation. Since these are linear and homogeneous equations, the function

$$\tilde{\psi}_{j,k}(x) = \exp[i\phi_j(k)]\psi_{j,k}(x) \tag{7}$$

describes the same normalized state as $\psi_{j,k}(x)$ does, provided $\phi_j(k)$ is a real function. Moreover, in agreement with Eq. (2), the phase shift $\phi_j(k)$ should satisfy

$$\phi_j(k+2\pi/a) - \phi_j(k) = 2r_j\pi, \tag{8}$$

with r_j being an integer. In these conditions, the Wannier function

$$\tilde{w}_j(x) = \frac{a}{2\pi}\int_{-\pi/a}^{\pi/a}\tilde{\psi}_{j,k}(x)dk = \frac{a}{2\pi}\int_{-\pi/a}^{\pi/a}\exp[i\phi_j(k)]\psi_{j,k}(x)dk \tag{9}$$

is not uniquely defined.[1,7] Therefore, given the Bloch states $\psi_{j,k}(x)$ in the first Brillouin zone, we may look for the function $\phi_j(k)$ which gives the maximally localized Wannier function (MLWF).[7]

We have found several localization criteria to measure the spread of the Wannier functions,[7,8] but we have chosen the variance of the probability distribution $|w_j(x)|^2$. The center and the variance of $|w_j(x)|^2$ are

$$x_j = \int_{-\infty}^{\infty}x|w_j(x)|^2dx \tag{10}$$

and

$$\sigma_j^2 = \int_{-\infty}^{\infty}(x-x_j)^2|w_j(x)|^2dx, \tag{11}$$

respectively. Moreover, σ_j is the standard deviation of $|w_j(x)|^2$. For short, we will refer to x_j, σ_j^2, and σ_j as parameters of the Wannier function $w_j(x)$.

In terms of the BFs, we obtain the center of $w_j(x)$ through Eqs. (4) and (10) as[11,12]

$$x_j = \langle X_j \rangle = \frac{a}{2\pi}\int_{-\pi/a}^{\pi/a}X_j(k)dk, \tag{12}$$

where

$$X_j(k) = i\int_0^a u_{j,k}^*(x)\frac{\partial u_{j,k}}{\partial k}(x)dx \tag{13}$$

and $u_{j,k}(x) = \exp(-ikx)\psi_{j,k}(x)$ is the periodic part of $\psi_{j,k}(x)$. From the normalization and periodicity of the BFs, it is quite easy to demonstrate that $X_j(k)$ is real and $X_j(k+2\pi/a) = X_j(k)$. It is interesting to note the $X_j(k)$ is the Berry connection of the jth band[12–14] and $2\pi x_j/a$ is the corresponding Berry phase.[9,13,15] Moreover, the variance of $w_j(x)$ may be expressed in terms of the BFs by substituting Eq. (4) into Eq. (11). This leads to [7]

$$\sigma_j^2 = \frac{a}{2\pi}\int_{-\pi/a}^{\pi/a}\int_0^a\left|\frac{\partial u_{j,k}}{\partial k}(x)\right|^2 dxdk - x_j^2. \tag{14}$$

A. Minimization of the variance

Let us suppose that, for a given j, we have $\psi_{j,k}(x)$ as a C^1 (continuously differentiable) function of k. A procedure to obtain Bloch functions of this kind is established in the next section. Moreover, let us shift the phase of the BFs by $\phi_j(k)$, according to Eqs. (7) and (8). To maintain the continuous differentiability of the BFs, we assume that $\phi_j'(k)$ is continuous. The new Bloch functions in Eq. (7) lead to a new Wannier function $\tilde{w}_j(x)$ in Eq. (9).

The center $\tilde{x}_j$ and the variance $\tilde{\sigma}_j^2$ of $\tilde{w}_j(x)$ are functionals of $\phi_j(k)$. In fact, from Eq. (13), we obtain the new Berry connection[13]

$$\tilde{X}_j(k) = X_j(k) - \phi_j'(k), \tag{15}$$

and Eq. (12) leads to the new center

$$\tilde{x}_j = x_j - r_j a. \tag{16}$$

Since r_j is an integer, we note that our phase shift may change the center of the Wannier function. However, such a change can only be an integer multiple of the lattice period.[11] Moreover, Eq. (14) leads to the new variance

$$\tilde{\sigma}_j^2 = \sigma_j^2 + x_j^2 - \tilde{x}_j^2 + \frac{a}{2\pi}\int_{-\pi/a}^{\pi/a}([\phi_j'(k)]^2 - 2X_j(k)\phi_j'(k))dk. \tag{17}$$

On the one hand, it is worth to note that $\tilde{\sigma}_j^2$ has no maximum value. In fact, due to the term $[\phi_j'(k)]^2$ in the integral, one may choose $\phi_j(k)$ to strongly vary within the Brillouin zone, thus giving as large a variance as required. On the other hand, we expect $\tilde{\sigma}_j^2$ has a minimum.

The phase shift $\phi_j(k)$ which minimizes $\tilde{\sigma}_j^2$ is obtained through the Calculus of Variations.[16] Let $\delta\phi_j(k)$ be a variation of $\phi_j(k)$. It should satisfy $\delta\phi_j(-\pi/a) = \delta\phi_j(\pi/a)$, in agreement with Eq. (8). This variation produces a first-order variation of $\tilde{\sigma}_j^2$ which is given by

$$\delta(\widetilde{\sigma}_j^2) = \frac{a}{\pi}\int_{-\pi/a}^{\pi/a}[\phi_j'(k) - X_j(k)]\delta\phi_j'(k)dk$$

$$= -\frac{a}{\pi}\int_{-\pi/a}^{\pi/a}[\phi_j''(k) - X_j'(k)]\delta\phi_j(k)dk, \qquad (18)$$

where an integration by parts has been performed. Now, when $\widetilde{\sigma}_j^2$ reaches its minimum value, the variation $\delta(\widetilde{\sigma}_j^2)$ should vanish, regardless the shape of $\delta\phi_j(k)$. This leads to the differential equation[12,16]

$$\phi_j''(k) = X_j'(k). \qquad (19)$$

Therefore, taking into account the boundary condition in Eq. (8) for $k = -\pi/a$ and Eq. (12), we obtain

$$\phi_j^{\mathrm{ML}}(k) = \phi_j^{\mathrm{ML}}(0) + r_j ak + \int_0^k[X_j(\bar{k}) - x_j]d\bar{k}. \qquad (20)$$

The Berry connection corresponding to a WF of minimum variance is obtained from Eqs. (15) and (20) as $\widetilde{X}_j^{\mathrm{ML}}(k) = x_j - r_j a$. This means that, when the Bloch states of the isolated band lead to the MLWF, the Berry connection is the constant $\widetilde{x}_j^{\mathrm{ML}} = x_j - r_j a$. Furthermore, the minimum variance is derived from Eqs. (18) and (20) as

$$\min(\widetilde{\sigma}_j^2) = \sigma_j^2 + x_j^2 - \frac{a}{2\pi}\int_{-\pi/a}^{\pi/a}X_j^2(k)dk = \sigma_j^2 + \langle X_j\rangle^2 - \langle X_j^2\rangle.$$

$$(21)$$

It should be noticed that this minimum value is less than or equal to σ_j^2, and does not depend on $\phi_j^{\mathrm{ML}}(0)$ or r_j in Eq. (20). This allows us to choose these latter parameters in the most convenient way.

B. Real Wannier functions

At this point we discuss whether, to obtain the MLWF, we may limit ourselves to deal with real Wannier functions. On the one hand, in agreement with Eq. (9), the MLWF may be written as

$$\widetilde{w}_j^{\mathrm{ML}}(x) = \frac{a}{2\pi}\int_0^{\pi/a}[\widetilde{\psi}_{j,k}^{\mathrm{ML}}(x) + \widetilde{\psi}_{j,-k}^{\mathrm{ML}}(x)]dk, \qquad (22)$$

where $\widetilde{\psi}_{j,k}^{\mathrm{ML}}(x) = \exp[i\phi_j^{\mathrm{ML}}(k)]\psi_{j,k}(x)$. On the other hand, we remind that $\psi_{j,-k}(x)$ and $\psi_{j,k}^*(x)$ are linearly dependent. Hence, there exists a real phase difference $\beta_j(k)$ between them, i.e.,

$$\psi_{j,-k}(x) = e^{i\beta_j(k)}\psi_{j,k}^*(x). \qquad (23)$$

Following Eq. (13), this leads to

$$X_j(-k) = X_j(k) + \beta_j'(k). \qquad (24)$$

Moreover, combining this result with Eq. (20), we obtain

$$\widetilde{\psi}_{j,-k}^{\mathrm{ML}}(x) = e^{2is_j}[\widetilde{\psi}_{j,k}^{\mathrm{ML}}(x)]^*, \qquad (25)$$

where $s_j = \phi_j^{\mathrm{ML}}(0) + \frac{1}{2}\beta_j(0)$. Therefore, we may rewrite Eq. (22) as

$$\widetilde{w}_j^{\mathrm{ML}}(x) = \frac{a}{2\pi}e^{is_j}\int_0^{\pi/a}[e^{-is_j}\widetilde{\psi}_{j,k}^{\mathrm{ML}}(x) + \mathrm{c.c.}]dk, \qquad (26)$$

This means that the maximally localized Wannier function equals a real function times $\exp(is_j)$. Furthermore, since this factor is physically meaningless, we adopt $s_j = 0$. Thus we obtain $\phi_j^{\mathrm{ML}}(0) = -\frac{1}{2}\beta_j(0)$ and

$$\widetilde{w}_j^{\mathrm{ML}}(x) = \frac{a}{\pi}\int_0^{\pi/a}\mathrm{Re}[\widetilde{\psi}_{j,k}^{\mathrm{ML}}(x)]dk. \qquad (27)$$

Since our MLWF belongs to the set of real Wannier functions, we may restrict the foregoing study to Bloch states leading to WFs in this set. To put it another way, the BFs will have the symmetry property

$$\psi_{j,-k}(x) = \psi_{j,k}^*(x). \qquad (28)$$

This is Eq. (23) with $\beta_j(k) = -2t_j\pi$ for an integer t_j. Hence, we obtain $\phi_j^{\mathrm{ML}}(0) = t_j\pi$, which should be substituted in Eq. (20). Here we point out that working with real Wannier functions is quite convenient in formal and numerical calculations, as well as for the graphical representations.

In addition, it should be noted that the phase shift $t_j\pi + r_j ak$, which consists of the first two terms on the right-hand side of Eq. (20), transforms $w_j(x)$ into $(-1)^{t_j}w_j(x+r_j a)$. Then, disregarding a possible but meaningless sign inversion, such a term does not affect the set of WFs of the jth band. For the sake of convenience and without losing generality, we shall use $t_j = 0$ and choose r_j as the integer part of $x_j/a + 1/2$. This way we will get $-a/2 < \widetilde{x}_j^{\mathrm{ML}} \le a/2$, i.e., the center of the MLWF will be in the unit cell centered at the origin.[11] We also note that the third term in Eq. (20) preserves the center and minimizes the variance of the Wannier function.

III. ENERGY BANDS AND BLOCH FUNCTIONS

In this section we develop the basic theory of energy bands and BFs in a quite general type of 1D crystal with lattice period a. We shall use a transfer-matrix formalism. Let the electronic motion be described by[3]

$$\hat{H} = -\frac{\hbar^2}{2}\frac{d}{dx}\frac{1}{m^*(x)}\frac{d}{dx} + V(x). \qquad (29)$$

The electron effective mass $m^*(x)$ is piecewise continuous and periodic, with period a. The effective potential $V(x)$ is taken as[6] $V(x) = V_s(x) + V_d(x)$, where $V_s(x)$ is piecewise continuous and periodic, with period a, and $V_d(x) = \frac{\hbar^2}{m_e a}\Sigma_{q,n}\alpha_q\delta(x - p_q - na)$, where $\delta(x)$ is the Dirac's delta. In this sum the index n takes all integer values and the positions p_q, with $0 \le p_q < a$, form a finite set. Moreover, each weight α_q may be positive or negative and m_e is the free-electron mass.

The eigenfunctions $\psi(x)$ of $\hat{H}$ should be continuous everywhere. Instead, for the considered effective potential, $\varphi(x) = am_e\psi'(x)/m^*(x)$ is piecewise continuous. In fact, $\varphi(x)$ is continuous everywhere except at $x = p_q + na$, with n being an integer. At such points the condition $\varphi(x^+) - \varphi(x^-)$

$=2\alpha_q\psi(x)$ applies. Here the superscripts $^+$ and $^-$ indicate lateral limits.

A. Transfer matrix

Let $\psi_{1,E}(x)$ and $\psi_{2,E}(x)$ be two real and linearly independent eigenfunctions of $\hat{H}$ for the eigenvalue E. Since the Schrödinger equation is a second-order linear differential equation, the general eigenfunction $\psi(x)$ for this eigenvalue may be written as

$$\psi(x) = C_1\psi_{1,E}(x) + C_2\psi_{2,E}(x). \tag{30}$$

For purposes of convenience and without losing generality, we assume[1,6]

$$\begin{pmatrix} \psi_{1,E}(x_0) & \psi_{2,E}(x_0) \\ \varphi_{1,E}(x_0^+) & \varphi_{2,E}(x_0^+) \end{pmatrix} = \begin{pmatrix} 1 & 0 \\ 0 & 1 \end{pmatrix}, \tag{31}$$

where the position x_0 may be chosen at will. Taking the values $\psi(x_0)$ and $\varphi(x_0^+)$ as initial conditions, we eliminate the constants C_1 and C_2 in Eq. (30) to obtain the transfer relation[3]

$$\begin{pmatrix} \psi(x) \\ \varphi(x^+) \end{pmatrix} = T(E;x,x_0)\begin{pmatrix} \psi(x_0) \\ \varphi(x_0^+) \end{pmatrix}, \tag{32}$$

where

$$T(E;x,x_0) = \begin{pmatrix} \psi_{1,E}(x) & \psi_{2,E}(x) \\ \varphi_{1,E}(x^+) & \varphi_{2,E}(x^+) \end{pmatrix} \tag{33}$$

is the transfer matrix from x_0 to x. As shown in Appendix A, its determinant is 1. Moreover, for real values of E, the matrix $T(E;x,x_0)$ is a real and C^∞ (infinite times differentiable[17]) function of E.

To obtain the Bloch states, we consider the primitive transfer matrix $M(E,x_0)=T(E;x_0+a,x_0)$. When the Bloch condition in Eq. (1) is taken into account, we get

$$M(E,x_0)\begin{pmatrix} \psi_k(x_0) \\ \varphi_k(x_0^+) \end{pmatrix} = e^{ika}\begin{pmatrix} \psi_k(x_0) \\ \varphi_k(x_0^+) \end{pmatrix}. \tag{34}$$

Since $\psi_k(x_0)$ and $\varphi_k(x_0^+)$ do not vanish simultaneously, this expression leads to the secular equation $\mu(E,x_0)=\cos(ka)$, where

$$\mu(E,x_0) = \frac{M_{11}(E,x_0) + M_{22}(E,x_0)}{2}. \tag{35}$$

This is one-half of the trace of $M(E,x_0)$, thus it does not depend on the initial position x_0. To show this, we write the primitive transfer matrix for the initial position x_0^0 as

$$\begin{aligned} M(E,x_0^0) &= T(E;x_0^0+a,x_0^0) \\ &= T(E;x_0^0+a,x_0+a)T(E;x_0+a,x_0)T(E;x_0,x_0^0) \\ &= T(E;x_0,x_0^0)M(E,x_0)T^{-1}(E;x_0,x_0^0). \end{aligned} \tag{36}$$

This is because $T(E;x_0^0+a,x_0+a)=T(E;x_0^0,x_0)$, due to the periodicity of the 1D crystal, and $T(E;x_0,x_0^0)=T^{-1}(E;x_0^0,x_0)$, as a consequence of Eq. (32). According to Eq. (36), $M(E,x_0)$ and $M(E,x_0^0)$ are similar matrices. Therefore, they
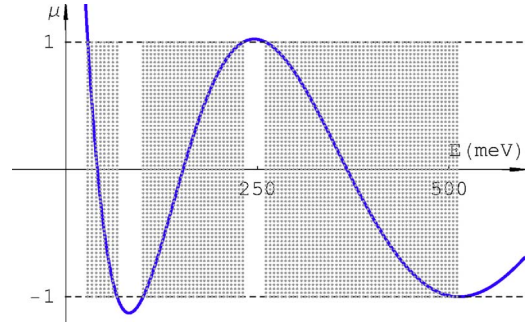

FIG. 1. (Color online) The Kramers plot of $\mu(E)$. The shaded regions indicate the lower three bands. The numerical values are for the structure SL2 in Sec. VIII.

have the same trace and we get $\mu(E,x_0)=\mu(E)$. Moreover, the secular equation becomes

$$\mu(E) = \cos(ka). \tag{37}$$

B. Properties of $\mu(E)$

For the purposes of the present work we note that, for real values of E, the function $\mu(E)$ is C^∞ everywhere.[17] Furthermore, we assume $\mu(E)$ has the following properties:[1]

$$\mu(E) \rightarrow +\infty \quad \text{as } E \rightarrow -\infty, \tag{38}$$

$$\text{if } \mu'(E)=0 \quad \text{then } E=E_l', \tag{39}$$

where E_l' is real and increases as $l=1,2,\ldots,$

$$|\mu_l| \geq 1, \tag{40}$$

where $\mu_l=\mu(E_l')$,

$$\text{sign}(\mu_l) = (-1)^j, \tag{41}$$

and

$$\text{sign}(\mu_l'') = (-1)^{l+1}. \tag{42}$$

where $\mu_l''=\mu''(E_l')$. Most of these properties are apparent in Fig. 1, where the Kramers plot of $\mu(E)$ is displayed.

C. Energy bands

According to Eq. (37), for a real k the energy E should satisfy $|\mu(E)| \leq 1$. Therefore, as the Kramers plot in Fig. 1 suggests, for each real k the secular equation has an infinite set of real roots $E_{j,k}$, where $j=1,2,\ldots$ increases with the energy value. For fixed j, the function $E_{j,k}$ gives the jth energy band. Such a function is continuous in the reciprocal space, with the periodicity

$$E_{j,k+2\pi/a} = E_{j,k} \tag{43}$$

and the inversion symmetry

$$E_{j,-k} = E_{j,k}. \tag{44}$$

Moreover, when the energies $E_{j,k}$ are nondegenerate, the jth band is isolated and $E_{j,k}$ is continuously differentiable.
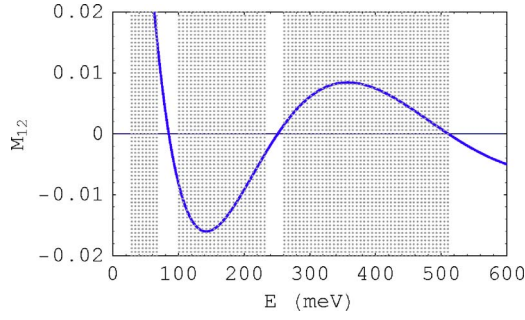
FIG. 2. (Color online) $M_{12}(E, x_0)$ as a function of E for fixed x_0. The shaded regions indicate the lower three bands. The numerical values are for the structure SL2 in Sec. VIII with $x_0 = 50$ Å.

D. Bloch functions

According to Eq. (32), the BFs are given by

$$\psi_{j,k}(x) = \psi_{j,k}(x_0) T_{11}(E_{j,k}; x, x_0) + \varphi_{j,k}(x_0^+) T_{12}(E_{j,k}; x, x_0),$$
(45)

where $\psi_{j,k}(x_0)$ and $\varphi_{j,k}(x_0^+)$ satisfy Eq. (34) and the normalization condition in Appendix B. If $M_{12}(E_{j,k}, x_0) \neq 0$ then Eq. (34) leads to

$$\varphi_{j,k}(x_0^+) = \frac{e^{ika} - M_{11}(E_{j,k}, x_0)}{M_{12}(E_{j,k}, x_0)} \psi_{j,k}(x_0).$$
(46)

Moreover, according to Eq. (B13), we get[1,3,6]

$$|\psi_{j,k}(x_0)| = \sqrt{-\frac{m_e a M_{12}(E_{j,k}, x_0)}{\hbar^2 \mu'(E_{j,k})}},$$
(47)

provided $\mu'(E_{j,k}) \neq 0$. However, the phase of the $\psi_{j,k}(x_0)$ remains undetermined. We shall fix this phase in a later section.

Similarly, when $M_{21}(E_{j,k}, x_0) \neq 0$ we may use Eq. (34) to get

$$\psi_{j,k}(x_0) = \frac{e^{ika} - M_{22}(E_{j,k}, x_0)}{M_{21}(E_{j,k}, x_0)} \varphi_{j,k}(x_0^+),$$
(48)

and Eq. (B14) leads to[3]

$$|\varphi_{j,k}(x_0^+)| = \sqrt{\frac{m_e a M_{21}(E_{j,k}, x_0)}{\hbar^2 \mu'(E_{j,k})}},$$
(49)

whenever $\mu'(E_{j,k}) \neq 0$.

E. Properties of $M_{12}(E, x_0)$ and $M_{21}(E, x_0)$

The off-diagonal elements $M_{12}(E, x_0) = \psi_{2,E}(x_0 + a)$ and $M_{21}(E, x_0) = \varphi_{1,E}(x_0 + a)$ play a central role in the calculation of the BFs. Therefore, we display some of their main properties in Figs. 2 and 3. For instance, the off-diagonal elements do not vanish inside the energy bands. Each of them has one zero per energy gap, and $M_{21}(E, x_0)$ vanishes once below the first band.

We assume that $M_{12}(E, x_0)$ and $M_{21}(E, x_0)$ have the following properties:

$$M_{12}(E, x_0) \to +\infty \quad \text{when } E \to -\infty,$$
(50)
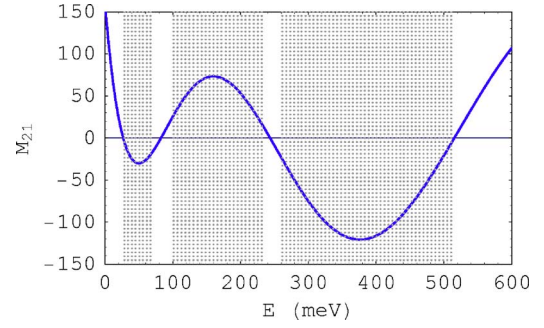

FIG. 3. (Color online) The same as Fig. 2, but here $M_{21}(E, x_0)$ is given as a function of E.

$$M_{21}(E, x_0) \to +\infty \quad \text{when } E \to -\infty,$$
(51)

$$\text{if } M_{12}(E, x_0) = 0 \quad \text{then } E = \bar{E}_l,$$
(52)

where $\bar{E}_l$ is real[1] and increases as $l = 1, 2, \dots$,

$$\text{if } M_{21}(E, x_0) = 0 \quad \text{then } E = \tilde{E}_l,$$
(53)

where $\tilde{E}_l$ is real and increases as $l = 0, 1, 2, \dots$. Here we point out that $\tilde{E}_0$ is below the first band. Moreover,

$$|\bar{\mu}_l| \geq 1 \quad \text{and} \quad |\tilde{\mu}_l| \geq 1,$$
(54)

with $\bar{\mu}_l = \mu(\bar{E}_l)$ and $\tilde{\mu}_l = \mu(\tilde{E}_l)$, and

$$M_{12}(E, x_0) = M_{21}(E, x_0) = 0$$

if and only if

$$|\mu(E)| = 1 \quad \text{and} \quad \mu'(E) = 0.$$
(55)

It is worth noting that, in such a case, E is a degenerate level which corresponds to a null gap. Furthermore,

$$\text{sign}\left(\frac{\partial M_{12}}{\partial E}(\bar{E}_l, x_0)\right) = \text{sign}(\bar{\mu}_l) = (-1)^l,$$
(56)

and

$$\text{sign}\left(\frac{\partial M_{21}}{\partial E}(\tilde{E}_l, x_0)\right) = -\text{sign}(\tilde{\mu}_l) = (-1)^{l+1}.$$
(57)

To explain Eq. (54) we point out that when one of the off-diagonal elements of $M(E, x_0)$ vanishes we have $M_{11}(E, x_0) M_{22}(E, x_0) = 1$ (see Appendix A). Thus $|M_{11}(E, x_0)| + |M_{22}(E, x_0)| \geq 2$, since the arithmetic mean is greater than or equal to the geometric mean. Moreover, $M_{11}(E, x_0)$ and $M_{22}(E, x_0)$ have the same sign. Therefore, we obtain $|\mu(E)| \geq 1$. In addition, the property in Eq. (55) can be seen as a consequence of Eqs. (B13) and (B14). To do so, we should bear in mind that $\psi_{j,k}(x_0)$ and $\varphi_{j,k}(x_0^+)$ cannot vanish simultaneously.

IV. THE FIRST STAGE

Here we obtain the Bloch function $\psi_{j,k}(x)$ of an isolated band as an everywhere continuously differentiable function

of the real wave number k. We recall that, for 1D crystals with inversion symmetry, Kohn[1] has conveniently chosen $x = 0$ as an inversion center. As a result, $x = a/2$ is also an inversion center. Then, depending on the band class,[3] one may choose $\psi_{j,k}(x_0) > 0$ or $\varphi_{j,k}(x_0) > 0$ for all real k, with x_0 being either 0 or $a/2$. In the present work we use the same idea, but, of course, x_0 needs not be an inversion-symmetry center.

The property in Eq. (55) guarantees that neither $\mu'(E) = 0$ nor $M_{12}(E, x_0)$ and $M_{21}(E, x_0)$ vanish simultaneously in an isolated band. To obtain $\psi_{j,k}(x)$ as a continuously differentiable function of k, it is convenient to use either Eqs. (46) and (47) or Eqs. (48) and (49) for the whole jth band. In the first case, we need $M_{12}(E_{j,k}, x_0) \neq 0$ to apply for all real k. Thus, according to Eq. (54), it is enough to choose x_0 such that the band edges ($E_{j,0}$ and $E_{j,\pi/a}$) are not zeros of $M_{12}(E, x_0)$. Instead, in the second case the condition $M_{21}(E_{j,k}, x_0) \neq 0$ should be fulfilled for all real k. Similarly, following Eq. (53), it suffices to choose x_0 such that $M_{21}(E, x_0)$ does not vanish at the band edges.

Let us consider the first case. According to Eq. (47), $\psi_{j,k}(x_0) \neq 0$ for all real k. Hence, the phase of the BFs may be fixed by choosing

$$\psi_{j,k}(x_0) = |\psi_{j,k}(x_0)| > 0 \tag{58}$$

for every real k. For short, the resulting Wannier function will be classified as a PψWF, where Pψ means positive-ψ. Here $|\psi_{j,k}(x_0)|$ and $\varphi_{j,k}(x_0^+)$ are given by Eqs. (47) and (46), respectively. The choice in Eq. (58) produces the BFs normalized to unity over the elementary unit cell and continuously differentiable functions of k. This is because $T(E; x, x_0)$, $M(E, x_0)$ and $\mu'(E)$ are continuously differentiable functions[17] of E, and $E_{j,k}$ depends smoothly on k.

Regarding the periodicity of the BFs in the reciprocal space, we first note that $\psi_{j,k+2\pi/a}(x_0) = \psi_{j,k}(x_0)$ and $\varphi_{j,k+2\pi/a}(x_0^+) = \varphi_{j,k}(x_0^+)$. This is obtained by combination of Eqs. (43), (46), and (47). Moreover, we follow Eqs. (43) and (45) to reach Eq. (2). The BFs also satisfy $\psi_{j,-k}(x_0) = \psi_{j,k}^*(x_0)$ and $\varphi_{j,-k}(x_0^+) = \varphi_{j,k}^*(x_0^+)$. This is due to Eqs. (44), (46), and (47), and because $M(E, x_0)$ is real for real E. Furthermore, this latter fact explains why the BFs in Eq. (45) satisfy Eq. (28). Therefore, in agreement with Sec. II, the PψWFs are real WFs.

In the second case Eq. (49) ensures $\varphi_{j,k}(x_0^+) \neq 0$ for all real k. Thus the phase of the BFs may be chosen such that

$$\varphi_{j,k}(x_0^+) = |\varphi_{j,k}(x_0^+)| > 0 \tag{59}$$

for every real k. For short, the resulting Wannier function will be classified as a PφWF, where Pφ means positive-φ. In this case $\psi_{j,k}(x_0)$ is derived through Eq. (48), and we also obtain BFs with the properties discussed in Sec. II.

Once $\psi_{j,k}(x_0)$ and $\varphi_{j,k}(x_0^+)$ have been obtained, the BFs and the WF are calculated by Eqs. (45) and (4), respectively. Moreover, Eqs. (12) and (14) may be used to determine the center x_j and standard deviation σ_j of $w_j(x)$. However, this stage will seldom produce a maximally localized WF.

V. THE SECOND STAGE

To optimize the localization of the Wannier function $\widetilde{w}_j(x)$, the phase of the BFs is shifted in $\phi_j^{\text{ML}}(k)$. This shift is obtained by Eq. (20), with r_j being the integer part of $x_j/a + 1/2$ and $\phi_j^{\text{ML}}(0) = 0$. The resulting BFs are denoted by $\widetilde{\psi}_{j,k}^{\text{ML}}(x)$ and the MLWF is calculated by Eq. (22). Moreover, the center of the MLWF satisfy $-a/2 < \widetilde{x}_j^{\text{ML}} \leq a/2$ and its variance is obtained through Eq. (21). It should be remarked that the MLWF produced in this stage does not depend on the initial position x_0. This is discussed in Appendix C.

VI. ASYMPTOTIC BEHAVIOR OF WANNIER FUNCTIONS

Kohn[1] and Eilenberger[6] have pointed out that one-dimensional Wannier functions can be exponentially localized. In doing so, they have considered the Bloch functions as analytic functions of the complex wave number k. Note that, contrasting this idea, k and E have been supposed to be real in the preceding sections of this paper. However, to develop the theory of the asymptotic behavior of WFs, we shall consider both of them as complex variables in this section.

A. Analytic continuation of energy bands

We first deal with the analytic continuation of the transfer matrix $T(E; x, x_0)$ into the complex E-plane. The resulting function of E have been shown to be entire,[1,6] provided $m^*(x)$ is constant and $V_d(x) = 0$. We expect this property remains for the Hamiltonian in Eq. (29). This way, the elements of the primitive transfer matrix $M(E, x_0)$ and its trace $\mu(E)$ are also entire functions over the whole E-plane. According to Eq. (39), the zeros of $\mu'(E)$ occur at the points E_l'. They are simple zeros which correspond to the minima and maxima in the Kramers plot.[1] Moreover, for an isolated band, we have $|\mu_l| > 1$. Therefore, E_l' belongs to the lth energy gap. When $m^*(x)$ is constant and $V_d(x) = 0$, it has been demonstrated that $\mu'(E)$ have no other zeros.[1,6] Again, we expect this applies for the Hamiltonian in Eq. (29).

Now we perform the analytic continuation of the energy bands by applying Eq. (37) for complex values of k and E. To obtain the bands, we should deal with the many-valued inverse of $\mu(E)$. Since the zeros of $\mu'(E)$ are simple, the values μ_l are first-order branch points of the function $E(\mu)$. For odd values of l the branch cut joins μ_l to $-\infty$ over the real axis of the μ-plane (with $\mu_l < -1$). In turn, for even values of l the branch cut joins μ_l to $+\infty$ over the same axis (with $\mu_l > 1$). The energy range of the jth band is produced by the branch $E_j(\mu)$ with $-1 \leq \mu \leq 1$. In fact, the points E_l' divide the real-E axis into a sequence of energy ranges, such that each range is produced by a different branch $E_j(\mu)$. For instance, the ranges $E \leq E_1'$ and $E_1' \leq E \leq E_2'$ are produced by the branches $E_1(\mu)$ and $E_2(\mu)$, respectively. Moreover, each branch corresponds to a Riemann sheet. The jth and the ($j+1$)th sheets are joined along the branch cut at μ_j. Hence, the complex-k bands are given by $E_{j,k} = E_j[\cos(ka)]$. We also note that such bands fulfill Eqs. (43) and (44).

Each complex-k band $E_{j,k}$ is analytic for all k, except for those k corresponding to the branch points and cuts of the branch $E_j(\mu)$. For $j=1$ the branch point is μ_1. In turn, for $j \geq 2$ the branch points are μ_{j-1} and μ_j. To find the k values corresponding to μ_l we remind the reader of Eq. (41) and set $k=k_1+ik_2$, where k_1 and k_2 are real numbers. Therefore, Eqs. (B2) and (B3) become

$$\cos(k_1 a) = (-1)^l \qquad (60)$$

and

$$\cosh(k_2 a) = |\mu_l|. \qquad (61)$$

This leads to the branch points[1]

$$k_{l,\nu,\pm} = \left(2\nu + \frac{1-(-1)^l}{2} \right) \frac{\pi}{a} \pm i h_l, \qquad (62)$$

where ν is an integer and

$$h_l = \frac{1}{a} \cosh^{-1}(|\mu_l|) = \frac{1}{a} \ln(|\mu_l| + \sqrt{\mu_l^2 - 1}). \qquad (63)$$

Moreover, each branch cut joins the point $k_{l,\nu,\pm}$ to $k_{l,\nu,\pm} \pm i\infty$. The branch points of $E_{1,k}$ are $k_{1,\nu,\pm}$. In turn, for $j \geq 2$, the branch points of $E_{j,k}$ are $k_{j-1,\nu,\pm}$ and $k_{j,\nu,\pm}$.

B. Analytic continuation of Bloch functions

The BFs for complex k are obtained by analytic continuation of the expressions in the preceding sections. To fix ideas, we deal with Bloch functions leading to a PψWF. As discussed in Sec. IV, we have

$$\psi_{j,k}(x) = \left(-\frac{m_e a M_{12}(E_{j,k}, x_0)}{\hbar^2 \mu'(E_{j,k})} \right)^{1/2} \left(T_{11}(E_{j,k}; x, x_0) \right.$$
$$\left. + T_{12}(E_{j,k}; x, x_0) \frac{e^{ika} - M_{11}(E_{j,k}, x_0)}{M_{12}(E_{j,k}, x_0)} \right), \qquad (64)$$

for real values of k. In this section, we use Eq. (64) for complex values of k as well. This expression clearly suggests that the branch points and cuts of $E_{j,k}$ apply to $\psi_{j,k}(x)$ as well. However, the BF may present additional branching properties, due to the zeros of $\mu'(E_{j,k})$ and $M_{12}(E_{j,k}, x_0)$.

The zeros of $\mu'(E_{j,k})$ occur at the branch points $k_{l,\nu,\pm}$ of $E_{j,k}$. Here $l=1$ and $l=j-1,j$ for $j=1$ and $j \geq 2$, respectively. In the neighborhood of those points we have $\mu(E_{j,k}) \approx \mu_l + \frac{1}{2}\mu_l''(E_{j,k}-E_l')^2$ and $\mu'(E_{j,k}) \approx \mu_l''(E_{j,k}-E_l')$. Therefore, we obtain

$$[\mu'(E_{j,k})]^2 \approx 2\mu_l''[\mu(E_{j,k}) - \mu_l]$$
$$= 2\mu_l''[\cos(ka) - \cos(k_{l,\nu,\pm}a)]$$
$$\approx -2\mu_l'' \sin(k_{l,\nu,\pm}a)(k - k_{l,\nu,\pm})$$
$$= 2|\mu_l''|\sinh(h_l a)[\pm ia(k - k_{l,\nu,\pm})], \qquad (65)$$

where we have used Eqs. (37), (42), and (62). We note that $\mu'(E_{j,k})$ has a first-order branch point at each $k_{l,\nu,\pm}$. The corresponding branch cut joins $k_{l,\nu,\pm}$ to $k_{l,\nu,\pm} \pm i\infty$. Moreover, in agreement with the Kramers plot, we obtain

$$\mu'(E_{j,k}) \approx (-1)^j \sqrt{2|\mu_l''|} \sinh(h_l a)[\pm ia(k - k_{l,\nu,\pm})] \quad (66)$$

for $k \approx k_{l,\nu,\pm}$.

According to Eq. (52), $M_{12}(E, x_0)$ vanishes at $E=\bar{E}_l$, with $l=1,2,\dots$. Then, following Eqs. (B2), (B3), (54), and (56), the complex wave numbers corresponding to $\bar{E}_l$ are

$$\bar{k}_{l,\nu,\pm} = \left(2\nu + \frac{1-(-1)^l}{2} \right) \frac{\pi}{a} \pm i\bar{h}_l, \qquad (67)$$

with

$$\bar{h}_l = \frac{1}{a} \ln(|\bar{\mu}_l| + \sqrt{\bar{\mu}_l^2 - 1}). \qquad (68)$$

It should be noted that $|\bar{\mu}_l| \leq |\mu_l|$, because $|\mu_l|$ is the maximum value of $\mu(E)$ in the lth gap. Consequently, $\bar{h}_l \leq h_l$ for all l. Moreover, Eq. (67) leads to

$$\exp(i k_{l,\nu,-} a) = \exp(-i k_{l,\nu,+} a). \qquad (69)$$

The function $\psi_{j,k}(x)$ can have additional branch properties at k values where $M_{12}(E_{j,k}, x_0)$ vanishes. However, the real energies produced by the first complex-k band are in the range $E \leq E_1'$. Hence, branch properties due to vanishing M_{12} occur in $\psi_{1,k}(x)$ when $\bar{E}_1 \leq E_1'$. For higher bands, the real energies of the jth complex-k band satisfy $E_{j-1}' \leq E \leq E_j'$. Therefore, additional branch properties occur in $\psi_{j,k}(x)$ when $E_{j-1}' \leq \bar{E}_{j-1}$ or $\bar{E}_j \leq E_j'$.

We now analyze the terms $M_{12}(E_{j,k}, x_0)$ and $\exp(ika) - M_{11}(E_{j,k}, x_0)$ in Eq. (64). To do so, we consider $k \approx \bar{k}_{l,\nu,\pm}$ and $\bar{E}_l$ in the jth complex-k band. According to Appendix D and Eq. (69), we have $\exp(i\bar{k}_{l,\nu,+}a) = M_{11}(\bar{E}_l, x_0)$ or $\exp(i\bar{k}_{l,\nu,-}a) = M_{11}(\bar{E}_l, x_0)$, depending on whether $|M_{11}(\bar{E}_l, x_0)| < 1$ or $|M_{11}(\bar{E}_l, x_0)| > 1$, respectively. This is because $|\exp(i\bar{k}_{l,\nu,\pm}a)| = \exp(\mp \bar{h}_l a)$.

For the sake of simplicity, we limit our discussion to the case $\bar{E}_l \neq E_l'$, where

$$E_{j,k} - \bar{E}_l \approx \left. \frac{dE_{j,k}}{dk} \right|_{k=\bar{k}_{l,\nu,\pm}} (k - \bar{k}_{l,\nu,\pm}) \qquad (70)$$

for $k \approx \bar{k}_{l,\nu,\pm}$. Hence, according to Eqs. (B4), (56), and (67), we have

$$M_{12}(E_{j,k}, x_0) \approx \frac{\partial M_{12}}{\partial E}(\bar{E}_l, x_0)[E_{j,k} - \bar{E}_l]$$
$$\approx -\frac{\sinh(\bar{h}_l a)}{\mu'(\bar{E}_l)} \left| \frac{\partial M_{12}}{\partial E}(\bar{E}_l, x_0) \right| [\pm ia(k - \bar{k}_{l,\nu,\pm})],$$
$$(71)$$

for $k \approx \bar{k}_{l,\nu,\pm}$. Moreover, if $\exp(i\bar{k}_{l,\nu,+}a) = M_{11}(\bar{E}_l, x_0)$ then
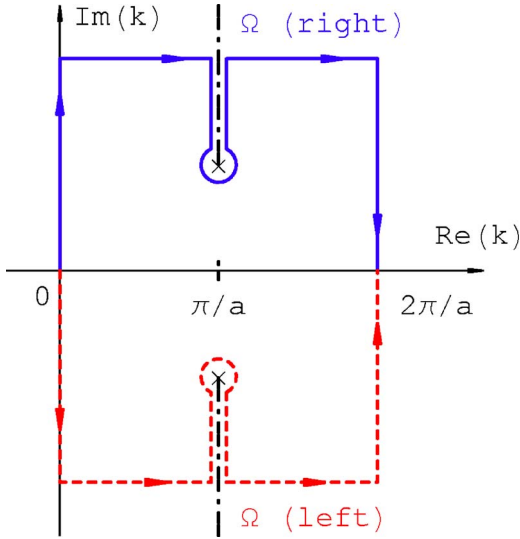
FIG. 4. (Color online) Branch points ($\times$), branch cuts (dotted-dashed lines) and integration path Ω in Eq. (76). The (blue) solid and the (red) dashed paths are used to find the asymptotic behavior of the PψWFs towards $+\infty$ and $-\infty$, respectively.

$$e^{ika} - M_{11}(E_{j,k}, x_0) \approx (-1)^l [ia(k - \bar{k}_{l,\nu,+})]$$
$$\times \left(e^{-\bar{h}_l a} + \frac{\sinh(\bar{h}_l a) \dfrac{\partial M_{11}}{\partial E}(\bar{E}_l, x_0)}{\mu'(\bar{E}_l)} \right)$$

(72)

for $k \approx \bar{k}_{l,\nu,+}$, and

$$e^{ika} - M_{11}(E_{j,k}, x_0) \approx 2i \sin(\bar{k}_{l,\nu,-}a) = 2(-1)^l \sinh(\bar{h}_l a).$$

(73)

for $k \approx \bar{k}_{l,\nu,-}$. Instead, if $\exp(i\bar{k}_{l,\nu,-}a) = M_{11}(\bar{E}_l, x_0)$ then

$$e^{ika} - M_{11}(E_{j,k}, x_0) \approx (-1)^l [-ia(k - \bar{k}_{l,\nu,-})]$$
$$\times \left(-e^{\bar{h}_l a} + \frac{\sinh(\bar{h}_l a) \dfrac{\partial M_{11}}{\partial E}(\bar{E}_l, x_0)}{\mu'(\bar{E}_l)} \right)$$

(74)

for $k \approx \bar{k}_{l,\nu,-}$, and

$$e^{ika} - M_{11}(E_{j,k}, x_0) \approx 2i \sin(\bar{k}_{l,\nu,+}a) = 2(-1)^{l+1} \sinh(\bar{h}_l a)$$

(75)

for $k \approx \bar{k}_{l,\nu,+}$.

C. Asymptotic behavior of positive-ψ Wannier functions

Here we obtain simple expressions for $w_1(x \pm ma)$ when m is a large positive integer. To do so, we approximate the integral in Eq. (4) by a suitable contour integral in the complex-k plane.[5] This involves an integral representation of the gamma function which is given in Appendix E.
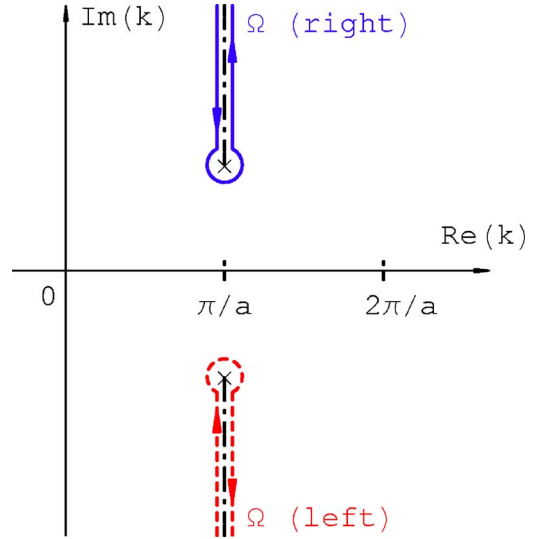

FIG. 5. (Color online) The same as Fig. 4, but the paths have been simplified.

According to Eq. (2), Eq. (4) is conveniently written as

$$w_j(x) = \frac{a}{2\pi} \int_0^{2\pi/a} \psi_{j,k}(x) dk = \frac{a}{2\pi} \int_\Omega \psi_{j,k}(x) dk, \quad (76)$$

where Ω is a path from 0 to $2\pi/a$ in the complex-k plane, and $\psi_{j,k}(x)$ is analytic in the region enclosed by Ω and the real-k axis.[5] To obtain the asymptotic behavior of the WF, the main advantage of this procedure comes from Eq. (1). Namely,

$$|\psi_{j,k}(x \pm ma)| = e^{\mp \text{Im}(k)ma} |\psi_{j,k}(x)|, \quad (77)$$

with m being a positive integer. The behavior of the Bloch function to the right-hand (left-hand) corresponds to the $+$ ($-$) sign in $x \pm ma$. To analyze the asymptotic behavior of the WF to the right-hand (left-hand) side we choose Ω in the region $\text{Im}(k) > 0$ [$\text{Im}(k) < 0$]. This is shown in Fig. 4. Hence, we obtain an exponential decay of $|\psi_{j,k}(x \pm ma)|$, as m increases, with coefficient $|\text{Im}(k)|$.

For the first band, we consider the following cases: (1) $\bar{E}_1 > E_1'$ and (2) $\bar{E}_1 < E_1'$. For simplicity, Ω is chosen in the region $0 \leq \text{Re}(k) \leq 2\pi/a$. It should be remarked that $\psi_{1,k}(x)$ is analytic for k in this region, with the exception of the branch points $k_{1,0,\pm} = \pi/a \pm ih_1$ and, in case 2, $\bar{k}_{1,0,\pm} = \pi/a \pm i\bar{h}_1$.

1. $\bar{E}_1 > E_1'$

In this case $\bar{E}_1$ is outside the first complex-k band. Thus the relevant branch points are $k_{1,0,\pm} = \pi/a \pm ih_1$. To determine the behavior of the WF on the right-hand side we use the (blue) solid path in Fig. 4. It should be noted that, according to Eq. (2), the vertical segments cancel out in Eq. (76). Therefore, for large positive values of m, the main contribution to $w_1(x + ma)$ comes from the vicinity of $k_{1,0,+}$. Moreover, for the same reason, the path Ω can be simplified to become the (blue) solid path in Fig. 5. In the simplified path

the vertical lines go to infinity.

According to Eqs. (64) and (66), we have

$$\psi_{1,k}(x + ma) \approx A_+(x)\exp(ikma)[ia(k - k_{1,0,+})]^{-1/4}, \quad (78)$$

when $k \approx k_{1,0,+}$. Here $A_+(x)$ is a real function which is defined for $-a/2 \leq x \leq a/2$. For large positive values of m, we make the substitution $t = -ima(k - k_{1,0,+})$. This way the (blue) solid path Ω in Fig. 5 becomes the Hankel contour in Appendix E. Moreover, Eq. (E1) is used to obtain[5,18]

$$w_1(x + ma) \approx \frac{A_{1,+}(x)}{\Gamma(\frac{1}{4})}(-1)^m \exp(-h_1 am)m^{-3/4}. \quad (79)$$

Furthermore

$$\psi_{1,k}(x - ma) \approx A_-(x)\exp(-ikma)[-ia(k - k_{1,0,-})]^{-1/4}, \quad (80)$$

when $k \approx k_{1,0,-}$, with $A_-(x)$ being a real function defined for $-a/2 \leq x \leq a/2$. To calculate $w_1(x - ma)$, we use the (red) dashed path in Fig. 4. This path simplifies to the (red) dashed path shown in Fig. 5, and we perform the substitution $t = ima(k - k_{1,0,-})$. This transforms the simplified Ω in the reverse of the Hankel contour in Appendix E, and we obtain

$$w_1(x - ma) \approx \frac{A_{1,-}(x)}{\Gamma(\frac{1}{4})}(-1)^m \exp(-h_1 am)m^{-3/4}. \quad (81)$$

We note that when $\bar{E}_1 > E_1'$ the WF is exponentially localized,[1] and present a power-law decay.[5] Moreover, both kinds of decay are isotropic. These properties have been already found in Wannier-Kohn functions of 1D crystals with inversion symmetry.[5]

2. $\bar{E}_1 < E_1'$

In this case, we focus the attention on the branch points $\bar{k}_{1,0,\pm}$. This is because the points $k_{1,0,\pm}$ are farther from the real-k axis, and its contribution to the integral should be negligible. Hence, we use the paths in Fig. 4 with branch points $\bar{k}_{1,0,\pm}$ and horizontal segments whose distance to real-k axis is less than h_j.

We consider the subcases: (2a) $|M_{11}(\bar{E}_j, x_0)| < 1$ and (2b) $|M_{11}(\bar{E}_j, x_0)| > 1$. In short, we present some details for case (2a). If $k \approx \bar{k}_{1,0,+} = \pi/a + i\bar{h}_1$ then Eqs. (64), (71), and (72) lead to

$$\psi_{1,k}(x + ma) \approx B_+(x)\exp(ikma)[ia(k - \bar{k}_{1,0,+})]^{1/2}. \quad (82)$$

In turn, when $k \approx \bar{k}_{1,0,-} = \pi/a - i\bar{h}_1$ we use Eqs. (64), (71), and (73) to obtain

$$\psi_{1,k}(x - ma) \approx B_-(x)\exp(-ikma)[-ia(k - \bar{k}_{1,0,-})]^{1/2}. \quad (83)$$

Here $B_\pm(x)$ are real functions defined for $-a/2 \leq x \leq a/2$. Hence, for large positive values of m, the integral along the (blue) solid path Ω in Fig. 4 gives

$$w_1(x + ma) \approx \frac{B_+(x)}{\Gamma(-\frac{1}{2})}(-1)^m \exp(-\bar{h}_1 am)m^{-3/2} \quad (84)$$

and integrating along the (red) dashed path we obtain

$$w_1(x - ma) \approx \frac{B_-(x)}{\Gamma(\frac{1}{2})}(-1)^m \exp(-\bar{h}_1 am)m^{-1/2}. \quad (85)$$

Similarly, in case (2b) we obtain

$$w_1(x + ma) \approx \frac{C_+(x)}{\Gamma(\frac{1}{2})}(-1)^m \exp(-\bar{h}_1 am)m^{-1/2} \quad (86)$$

and

$$w_1(x - ma) \approx \frac{C_-(x)}{\Gamma(-\frac{1}{2})}(-1)^m \exp(-\bar{h}_1 am)m^{-3/2} \quad (87)$$

for large positive values of m. The real functions $D_\pm(x)$ are defined for $-a/2 \leq x \leq a/2$.

For $\bar{E}_1 < E_1'$ we have obtained interesting results. On the one hand, the exponential decay occurs with coefficient $\bar{h}_1$, which is less than h_1. This reduction of the exponential localization has been already commented on by Prodan.[10] On the other hand, the power-law decay is anisotropic. These properties will be illustrated below.

D. Exponential and power-law localization

We have obtained the asymptotic behavior of PψWFs of the first band. In case 1 ($\bar{E}_1 > E_1'$) the exponential and power-law decays are isotropic. In turn, in case 2 ($\bar{E}_1 < E_1'$) the exponential decay is reduced and the power-law decay is anisotropic. To unify these results we write

$$|w_1(x \pm ma)| \approx G_\pm(x)\exp(-\eta m)m^{-\alpha_\pm}, \quad (88)$$

where $G_\pm(x)$ are positive functions defined for $-a/2 \leq x \leq a/2$. In case 1 we obtain $\eta = h_1 a$ and $\alpha_\pm = 3/4$. Instead, in case 2 we obtain $\eta = \bar{h}_1 a$. Moreover, in case (2a) [(2b)] α_+ is 3/2 (1/2) and α_- is 1/2 (3/2).

To study the localization of the Wannier functions, we use the probability

$$P_m = \int_{-a/2}^{a/2} |w_1(x + ma)|^2 dx \quad (89)$$

to find the electron with $(m - \frac{1}{2})a \leq x \leq (m + \frac{1}{2})a$. Moreover, we take an initial position x_0 leading to a WF whose center x_1 satisfies $-a/2 < x_1 \leq a/2$. Hence, for large positive values of m we obtain

$$P_{\pm m} \approx \exp(-2\eta m)m^{-2\alpha_\pm} \int_{-a/2}^{a/2} G_\pm^2(x)dx \quad (90)$$

and

$$\frac{1}{2}\ln\left(\frac{P_{\pm m}}{P_{\pm(m+1)}}\right) \approx \eta + \alpha_\pm \ln\left(1 + \frac{1}{m}\right). \quad (91)$$

We shall use this expression to determine the values of η and $\alpha_\pm$ from the numerical calculations.

In this section we have dealt with the PψWFs of the first band. For higher bands ($j \geq 2$), the same ideas apply, but we should consider branch points corresponding to energies in the two neighboring gaps. Moreover, the asymptotic behavior is dominated by the slower exponential decay. If $\bar{E}_{j-1} < E'_{j-1}$ and $E'_j < \bar{E}_j$ then the coefficient η of the exponential decay will be the smaller value between $h_{j-1}a$ and $h_j a$. This is in agreement with Kohn's theory.[1,3,5] Instead, in other cases, η may be $\bar{h}_{j-1}a$ or $\bar{h}_j a$. Furthermore, we have discussed the properties of the PψWFs thoroughly, but similar ideas apply to PφWFs. In such a case the off-diagonal element $M_{21}(E_{j,k}, x_0)$ plays a central role.

VII. THE INVERSION SYMMETRY

Our theory applies to 1D crystals with or without inversion symmetry. Since the former case has been successfully approached in the literature,[1,3] it is important to consider it in some detail.

If both $m^*(x)$ and $V(x)$ are symmetric about the point $x = x_s$, i.e., $m^*(x_s - x) = m^*(x_s + x)$ and $V(x_s - x) = V(x_s + x)$, then the crystal has inversion symmetry at this point. Due to this symmetry, the Bloch functions produced in the first stage have the property[6]

$$\psi_{j,-k}(x_s - x) = \exp[i\gamma_j(k)]\psi_{j,k}(x_s + x), \quad (92)$$

where $\gamma_j(k)$ is real and satisfies $\gamma_j(k + 2\pi/a) - \gamma_j(k) = 2\rho_j \pi$ and $\gamma_j(-k) + \gamma_j(k) = 2\tau_j \pi$, with ρ_j and τ_j being integer numbers. Then, using Eqs. (13) and (12), we obtain

$$X_j(k) = x_s + \frac{1}{2}\gamma'_j(k) \quad (93)$$

and $x_j = x_s + \rho_j a/2$, respectively. It should be noted that, in this case, the center x_j of $w_j(x)$ is a point of inversion symmetry of the crystal.

Now, to obtain the MLWF, we perform the second stage. The phase shift leading to WFs of minimum variance is given by Eq. (20) as

$$\phi_j^{\mathrm{ML}}(k) = t_j \pi + r_j ak + \frac{\gamma_j(k) - \tau_j \pi - \rho_j ak}{2}. \quad (94)$$

Hence, in agreement with Eq. (92), we find

$$\tilde{\psi}_{j,-k}^{\mathrm{ML}}(x_0 - x) = (-1)^{\tau_j}\tilde{\psi}_{j,k}^{\mathrm{ML}}(x_0 + x), \quad (95)$$

where $x_0 = x_j - r_j a$ is the center of $\tilde{w}_j^{\mathrm{ML}}(x)$. The 1D crystal has inversion symmetry about this point. In addition, according to Eqs. (9) and (95),

$$\tilde{w}_j^{\mathrm{ML}}(x_0 - x) = (-1)^{\tau_j}\tilde{w}_j^{\mathrm{ML}}(x_0 + x), \quad (96)$$

i.e., the MLWF is real and symmetric or antisymmetric about the point x_0, for even and odd values of τ_j, respectively. Therefore, the MLWF should be the Wannier-Kohn function.[1–3,6]

It is interesting to note that in 1D crystals with inversion symmetry the MLWF may be chosen as[3] either a PψWF or a PφWF (see Sec. IV). Thus we may wonder whether the same
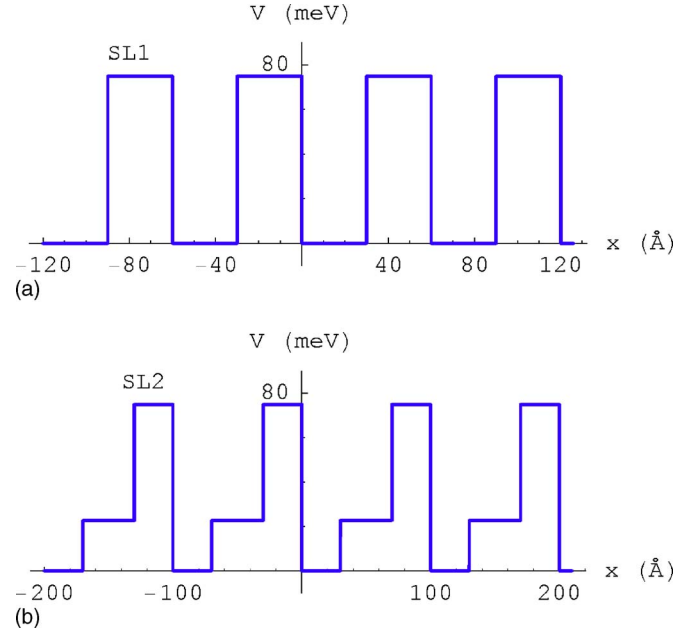

FIG. 6. (Color online) The potential profiles for the structures (a) SL1 and (b) SL2.

applies when the 1D crystal lacks inversion symmetry. If the answer were positive, then we would obtain the MLWF by appropriately choosing the initial position x_0. Such a choice would substitute the second stage. Additionally, this would help to analytically predict the asymptotic behavior of the MLWF.

VIII. NUMERICAL RESULTS

To illustrate the present theory, we deal with conduction electrons in periodic superlattices (SLs) grown along the x-axis direction.[3] We use the effective-mass approximation, where the transversal motion is free and, for simplicity, we set $k_y = k_z = 0$. Therefore, the electronic states can be described by the Hamiltonian in Eq. (29).

We consider two superlattices, which are denoted by SL1 and SL2. The unit cell of SL1 is AB, where A and B are 30 Å GaAs and 30 Å Ga$_{0.9}$Al$_{0.1}$As slabs, respectively. In this case, the crystal has period 60 Å and presents inversion symmetry. In turn, the unit cell of SL2 is ACB, with C being a 40 Å Ga$_{0.97}$Al$_{0.03}$As layer. Therefore, SL2 lacks inversion symmetry and has period 100 Å. In both cases, the position $x = 0$ is chosen at the left-hand interface of layer A. Moreover, in terms of the Al concentration c_l in the lth layer,[3] we use the effective mass $m^*/m_e = m_l = 0.067 + 0.083c_l$ and the effective potential $V_l = 748.2c_l$ meV. The potential profiles for the structures SL1 and SL2 are depicted in Fig. 6.

These layered systems are suitable to deal with different values of the initial position x_0. However, the general form of the transfer matrices is quite cumbersome. Therefore, we give the main principles only. On the one hand, using Eq. (32) for arbitrary positions x_1, x_2, and x_3, we have

$$T(E; x_3, x_1) = T(E; x_3, x_2)T(E; x_2, x_1). \quad (97)$$

On the other hand, when x_1 and $x_2 = x_1 + \Delta x$ are in the lth layer, we get
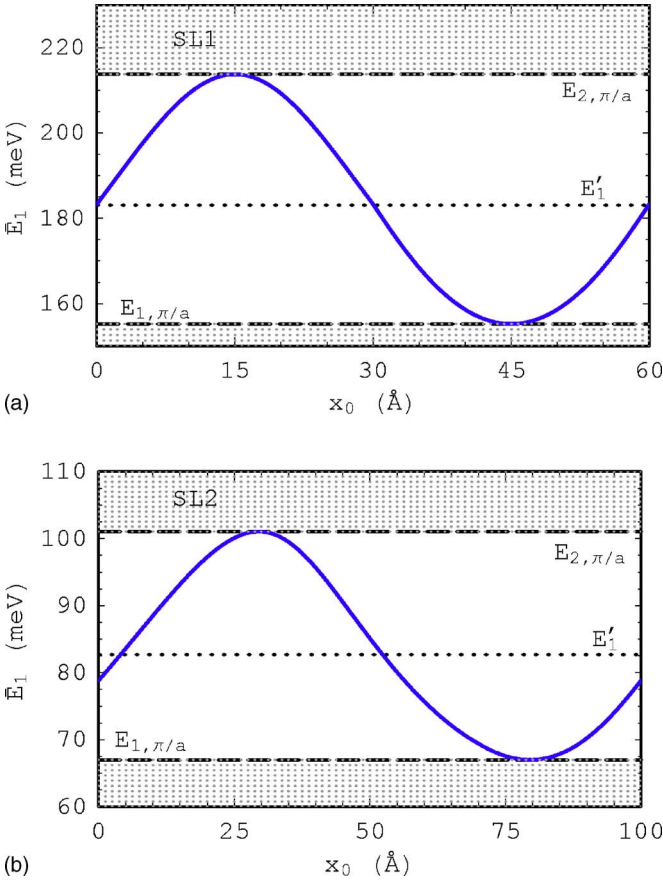
(a)

(b)

FIG. 7. (Color online) The first root $\bar{E}_1$ of $M_{12}(E,x_0)=0$, as a function of the initial position x_0 in the structures (a) SL1 and (b) SL2. The shaded regions correspond to the first and the second bands.

$$T(E;x_2,x_1) = \begin{pmatrix} \cos(q_l\Delta x) & \dfrac{m_l}{aq_l}\sin(q_l\Delta x) \\[2ex] -\dfrac{aq_l}{m_l}\sin(q_l\Delta x) & \cos(q_l\Delta x) \end{pmatrix}, \quad (98)$$

where $q_l=\sqrt{2m_e m_l(E-V_l)/\hbar^2}$.

For each structure, the energy bands have been calculated for a set of 400 equally spaced values of k in the first Brillouin zone. Moreover, following Eq. (4), the Wannier functions are obtained by numerical integration of the Bloch functions. Further details on the numerical procedures will be given elsewhere.

A. One-dimensional crystal with inversion symmetry

We first deal with the structure SL1, which presents inversion symmetry, as clearly shown in Fig. 6(a). The edges of the first band are $E_{1,0}\approx 35.46$ meV and $E_{1,\pi/a}\approx 155.2$ meV, respectively. In turn, the edges of the second band are $E_{2,\pi/a}\approx 213.8$ meV and $E_{2,0}\approx 626.6$ meV, respectively. Moreover, the first gap is the energy range $E_{1,\pi/a}\leq E\leq E_{2,\pi/a}$ and $E_1'\approx 183.1$ meV. Figure 7(a) displays $\bar{E}_1$ as a function of the initial position x_0, with $0\leq x_0\leq a$. Of course, $\bar{E}_1$ is a periodic function of x_0, with period a. It
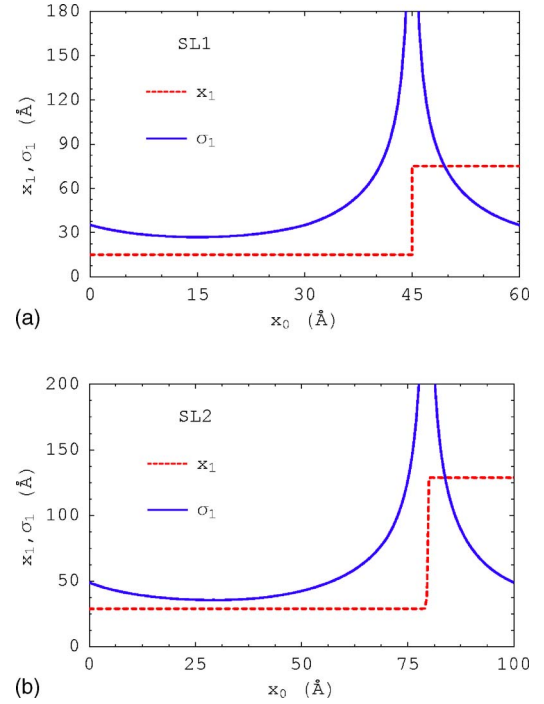

(a)

(b)

FIG. 8. (Color online) The center [(red) dashed line] and standard deviation [(blue) solid line] of the positive-ψ Wannier functions of the first band, in terms of the initial position x_0 in the structures (a) SL1 and (b) SL2.

should be noticed that $\bar{E}_1$ oscillates between the edges of the first gap. On the one hand, $\bar{E}_1=E_{1,\pi/a}$ when $x_0=45$ Å. Hence, we have $M_{12}(E_{1,k},x_0)\neq 0$ for all real-k, provided $x_0\neq (45+60n)$ Å for all integer values of n. On the other hand, $\bar{E}_1=E_{2,\pi/a}$ when $x_0=15$ Å.

Before the calculation of specific Wannier functions, let us analyze the parameters of the PψWFs. Equations (12) and (14) are used to obtain the dependence of the center and the standard deviation of $w_1(x)$ on the initial position x_0. The results for the structure SL1 are displayed in Fig. 8(a). The center x_1 follows a staircase law, with onsets at $(45+60n)$ Å, where n is an integer. In fact, the center increases in a when we use the initial position x_0+a instead of x_0. Moreover, due to the translational invariance, the standard deviation σ_1 is periodic in x_0, with period $a=60$ Å. The σ_1 tends to infinity as $x_0\to(45+60n)$ Å and attains its minimum value 26.91 Å (as a function of x_0) at $x_0=(15+60n)$ Å. In fact, such initial positions produce the MLWF.[1,3]

We have chosen the initial positions $x_0=20$ Å and $x_0=40$ Å to study the PψWFs. This choice is based on Fig. 8(a). Namely, $\bar{E}_1\approx 209.3$ meV $>E_1'$ for $x_0=20$ Å and $\bar{E}_1\approx 158.6$ meV $<E_1'$ for $x_0=40$ Å. Therefore, $x_0=20$ Å and $x_0=40$ Å will illustrate the two kinds of asymptotic behavior discussed in Sec. VI. Moreover, Fig. 8(a) shows that both initial positions lead to PψWFs centered at $x_1=15$ Å. Since $a=60$ Å, we have $-a/2<x_1\leq a/2$, in agreement with Sec. VI D.

Wannier functions of the first band in the structure SL1 are displayed in Fig. 9. The PψWFs, which are obtained in the first stage for $x_0=20$ Å and $x_0=40$ Å, are the (red)
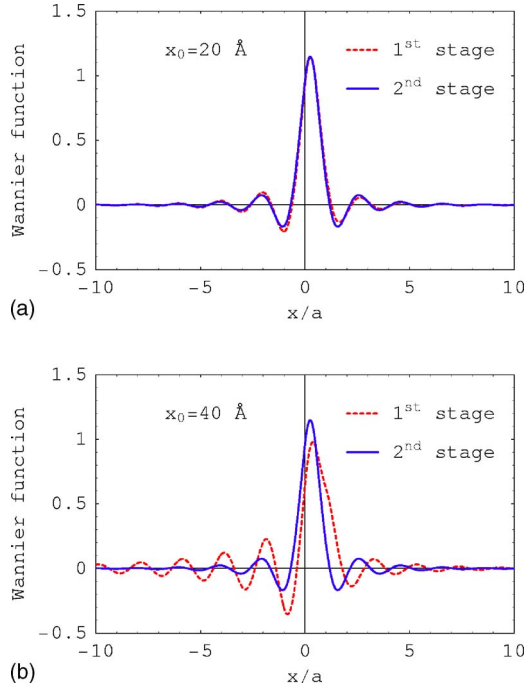
FIG. 9. (Color online) Wannier functions, in units of $1/\sqrt{a}$, of the first band in the structure SL1. The initial position x_0 is 20 Å and 40 Å in (a) and (b), respectively. The (red) dashed [(blue) solid] line is the PψWF (MLWF).

FIG. 10. (Color online) Probability P_m, for an electron in the Wannier state of the first band of the structure SL1 to be found with $(m-\frac{1}{2})a \leq x \leq (m+\frac{1}{2})a$, as a function of m. The initial position is 20 Å and 40 Å in (a) and (b), respectively. The (red) diamonds [(blue) squares] are for the PψWF (MLWF).

dashed lines in Figs. 9(a) and 9(b), respectively. Moreover, the (blue) solid line represents the MLWF obtained in the second stage. In agreement with Appendix C, the MLWF is the same for the two values of x_0. We observe that all these Wannier functions are quite well localized around their common center $x_1 = 15$ Å. In fact, the standard deviations of the PψWFs with $x_0 = 20$ Å and $x_0 = 40$ Å, are $\sigma_1 \approx 27.69$ Å and $\sigma_1 \approx 70.83$ Å, respectively. In turn, the standard deviation of the MLWF is $\tilde{\sigma}_1^{ML} \approx 26.91$ Å. It should be noted that the maximally localized WF in this symmetric structure is a PψWF.[1,3] In fact, it is the PψWF for $x_0 = 15$ Å, which is a point of inversion symmetry of the 1D crystal.

The exponential localization of the Wannier functions is apparent in Fig. 10, where the natural logarithm of the probability P_m is displayed as a function of the cell index m. In fact, $\ln(P_m)$ varies almost linearly with m, for large values of $|m|$. Here we remind the reader that P_m is defined by Eq. (89) and gives the probability for an electron, in a Wannier state of the first band, to be found with $(m-\frac{1}{2})a \leq x \leq (m+\frac{1}{2})a$. The (red) diamonds show the results for the PψWFs with $x_0 = 20$ Å and $x_0 = 40$ Å, respectively. Since the slopes are larger for $x_0 = 20$ Å than for $x_0 = 40$ Å, the PψWF is more localized in the former case. This is in agreement with Fig. 9. Moreover, the PψWF for $x_0 = 40$ Å show some degree of anisotropy. Namely, the decay to the right-hand side seems to be faster than to the left-hand side. Furthermore, the (blue) squares correspond to the MLWF. It nearly reproduces the behavior of the PψWF for $x_0 = 20$ Å.

For a quantitative analysis of the asymptotic behavior of the Wannier functions, we display in Fig. 11 one-half of $\ln(P_{\pm m}/P_{\pm(m+1)})$ as a function of $\ln(1+1/m)$. The (red) dia-
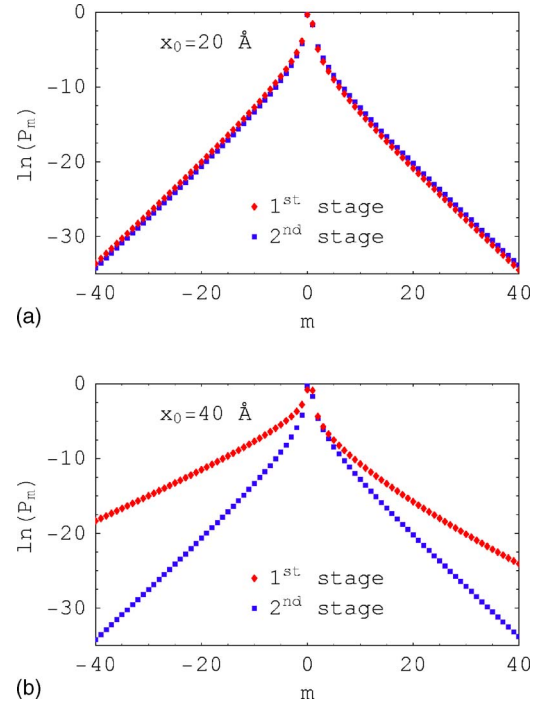
monds [(blue) squares] correspond to the $-$ (+) sign, and show the behavior of the WF to the left-hand (right-hand) side. Clearly, the results are in agreement with Eq. (91). Figure 11(a) shows the results for the PψWF with $x_0 = 20$ Å. Since $\bar{E}_1 > E_1'$, they correspond to Eqs. (79) and (81) in Sec. VI. The coefficient of the exponential decay is given by Eq. (63), i.e., $\eta = h_1 a \approx 0.3129$. Moreover, the slopes of the isotropic power-law decay are $\alpha_{\pm} = 3/2$.

More interestingly, the results for the PψWF with $x_0 = 40$ Å are shown in Fig. 11(b). In this case we observe both a reduction of the exponential coefficient[10] and the anisotropic power-law decay with exponents $\alpha_+ = 3/2$ (to the right-hand side) and $\alpha_- = 1/2$ (to the left-hand side). Since $\bar{E}_1 < E_1'$ and $M_{11}(\bar{E}_1, x_0) \approx -0.8587$, these results correspond to Eqs. (84) and (85), respectively. The reduced exponential coefficient is given by Eq. (68), i.e., $\eta = \bar{h}_1 a \approx 0.1524$.

The results for the MLWF are displayed in Fig. 11(c). Indeed, it is the PψWF for $x_0 = 15$ Å, with $\bar{E}_1 \approx 213.8$ meV $> E_1'$. Therefore, it has the same asymptotic behavior as the PψWF shown in Fig. 11(a). This is the expected result for the MLWF in a 1D crystal with inversion symmetry.[5]

B. One-dimensional crystal without inversion symmetry

Now we deal with the structure SL2, which lacks inversion symmetry, as may be observed in Fig. 6(b). The edges of the first band are $E_{1,0} \approx 28.81$ meV and $E_{1,\pi/a} \approx 66.99$ meV, respectively. In turn, the edges of the second band are $E_{2,\pi/a} \approx 101.1$ meV and $E_{2,0} \approx 231.2$ meV, respec-
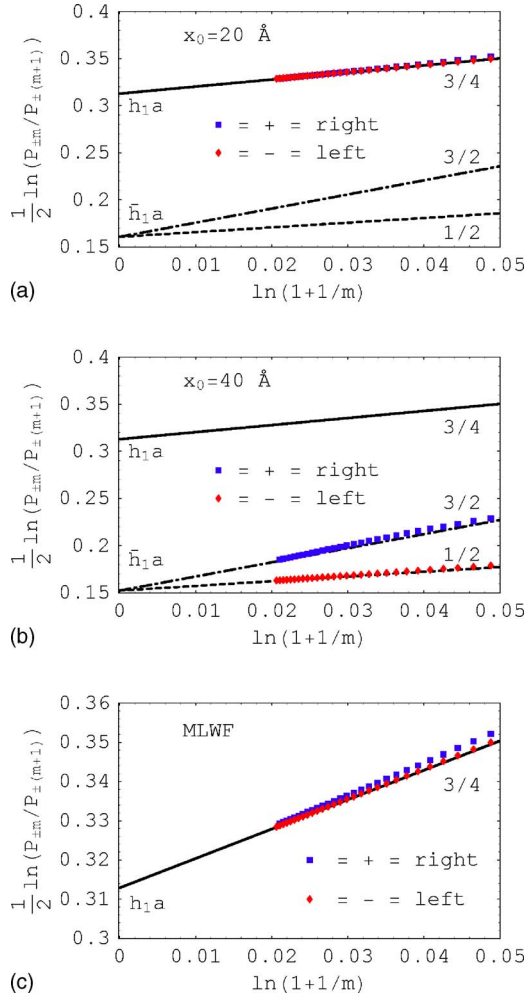
(a)

(b)

(c)

FIG. 11. (Color online) One-half of the natural logarithm of the ratio between the probabilities for an electron, in the Wannier state of the first band of the structure SL1, to be found in the $\pm m$th and $\pm(m+1)$th cells as a function of $\ln(1+1/m)$. Panel (a) [(b)] corresponds to the PψWF with $x_0=20$ Å ($x_0=40$ Å). Panel (c) is for the MLWF. The (blue) squares [(red) diamonds] are for the $+$ ($-$) sign and display the asymptotic behavior to the right-hand (left-hand) side. The slopes of the dashed, solid, and dotted-dashed lines are 1/2, 3/4, and 3/2, respectively.

tively. Moreover, the first gap is the energy range $E_{1,\pi/a}$ $\leq E \leq E_{2,\pi/a}$ and $E_1' \approx 82.68$ meV. Figure 7(b) displays $\bar{E}_1$ as a function of the initial position x_0, with $0 \leq x_0 \leq a$. Again, $\bar{E}_1$ is a periodic function of x_0, with period a. As in the symmetric crystal, $\bar{E}_1$ oscillates between the edges of the first gap. It touches the first band at $E_{1,\pi/a}$ when $x_0 \approx 79.52$ Å. For other initial positions the off-diagonal element $M_{12}(E_{j,k},x_0)$ does not vanish. Furthermore, $\bar{E}_1 = E_{2,\pi/a}$ when $x_0 \approx 29.57$ Å.

As for SL1, we first analyze the parameters x_j and σ_j of the PψWFs. The results for the structure SL2 are displayed in Fig. 8(b). The center x_1 is piecewise constant and has the discontinuity near 79.52 Å. Moreover σ_j tends to infinity as $x_0 \rightarrow 79.52$ Å. The minimum σ_1, as a function of x_0, is about 35.46 Å, and occurs near $x_0=29.57$ Å.

In the structure SL2 we have chosen $x_0=40$ Å and $x_0 =70$ Å as initial positions to study the PψWFs. Such a choice
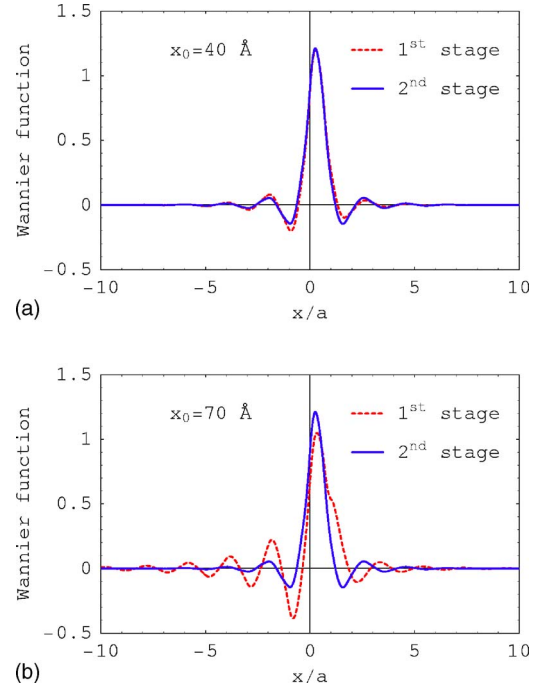

(a)

(b)

FIG. 12. (Color online) The same as Fig. 9, but for the structure SL2. Moreover, x_0 is 40 Å and 70 Å in (a) and (b), respectively.

is based on Fig. 7(b). On the one hand, $\bar{E}_1 \approx 95.67$ meV $> E_1'$ for $x_0=40$ Å. On the other hand, $\bar{E}_1 \approx 69.43$ meV $< E_1'$ for $x_0=70$ Å. Hence, these initial positions will illustrate the two kinds of asymptotic behavior discussed in Sec. VI. Furthermore, Fig. 8(b) shows that both values of x_0 lead to PψWFs centered at $x_1 \approx 28.87$ Å. Since $a=100$ Å, we have $-a/2 < x_1 \leq a/2$, in agreement with Sec. VI D.

Figure 12 displays Wannier functions of the first band in the structure SL2. The PψWFs for $x_0=40$ Å and $x_0=70$ Å are the (red) dashed lines in Figs. 12(a) and 12(b), respectively. In turn, the MLWF is the (blue) solid line. All these Wannier functions are centered at $x_1 \approx 28.87$ Å. Moreover, the standard deviations of the PψWFs with $x_0=40$ Å and $x_0=70$ Å, are $\sigma_1 \approx 37.07$ Å and $\sigma_1 \approx 82.47$ Å, respectively. The standard deviation of the MLWF is $\tilde{\sigma}_1^{ML} \approx 35.46$ Å. It is worthy to notice that the maximally localized WF in this nonsymmetric structure seems to be a PψWF. In fact, within the limits of our numerical calculations, it is the PψWF for the initial position $x_0 \approx 29.57$ Å. Interestingly, this is the initial position where $\bar{E}_1$ takes its maximum value $E_{2,\pi/a}$ in Fig. 7(b).

The exponential localization of the Wannier functions in the structure SL2 is clearly seen in Fig. 13. There, the natural logarithm of the probability P_m is displayed as a function of the cell index m. Note that $\ln(P_m)$ varies almost linearly with m, for large values of $|m|$. The (red) diamonds show the results for the PψWFs with $x_0=40$ Å and $x_0=70$ Å, respectively. In agreement with Fig. 12, the slopes for $x_0=40$ Å are larger, i.e., the corresponding PψWF is much more localized. Moreover, regarding the PψWF with $x_0=70$ Å in Fig. 13(b), the decay to the right-hand side seems to be faster than to the left-hand side. The (blue) squares correspond to the MLWF. It resembles the PψWF with $x_0=40$ Å.
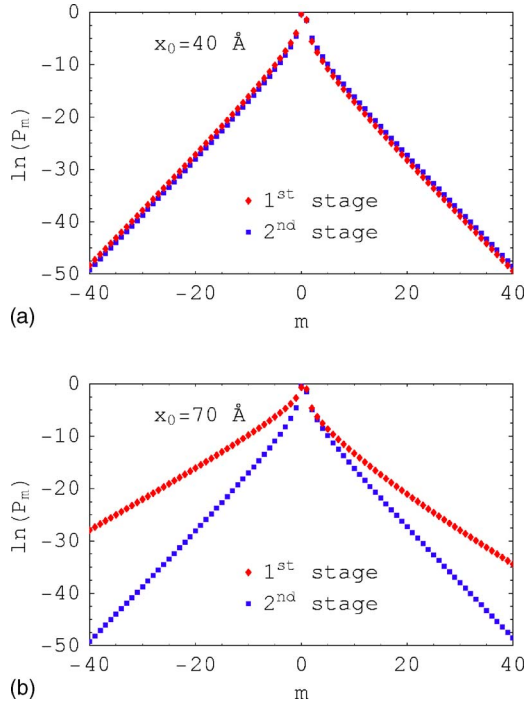
(a)

(b)

FIG. 13. (Color online) The same as Fig. 10, but for the structure SL2. Moreover, x_0 is 40 Å and 70 Å in (a) and (b), respectively.

We now analyze the asymptotic behavior of the Wannier functions quantitatively. Taking into account Eq. (91), one-half of $\ln(P_{\pm m}/P_{\pm(m+1)})$ is shown as a function of $\ln(1+1/m)$ in Fig. 14. Figure 14(a) shows the results for the $P\psi$WF with $x_0=40$ Å. Since $\bar{E}_1 > E'_1$, it corresponds to Eqs. (79) and (81) in Sec. VI. Note that the power-law decay is isotropic with $\alpha_{\pm}=3/4$. Moreover, the coefficient of the exponential decay is given by Eq. (63), i.e., $\eta=h_1 a \approx 0.5020$.

The results for the $P\psi$WF with $x_0=70$ Å are shown in Fig. 14(b). The exponential coefficient η is reduced,[10] in comparison with Fig. 14(a), and the power-law decay is anisotropic. Since $\bar{E}_1 < E'_1$ and $M_{11}(\bar{E}_1,x_0) \approx -0.7573$, these results correspond to Eqs. (84) and (85), respectively. The reduced exponential coefficient is given by Eq. (68), i.e., $\eta = \bar{h}_1 a \approx 0.2780$, and the power-law exponents are $\alpha_{+}=3/2$ (to the right-hand side) and $\alpha_{-}=1/2$ (to the left-hand side).

Within our numerical precision, the MLWF of the first band in SL2 is the $P\psi$WF for $x_0 \approx 29.57$ Å. Since $\bar{E}_1 \approx 101.1$ meV $> E'_1$, it satisfies Eqs. (79) and (81), in agreement with Fig. 14(c). We suspect this is a general property of the MLWF of isolated bands in a noncentrosymmetric 1D crystal.[5]

IX. CONCLUSIONS

We have dealt with Bloch and Wannier functions of isolated bands in 1D crystals with or without inversion symmetry. First, we obtained the phase shift one should perform on the Bloch functions to obtain the maximally localized Wannier functions. Such a shift was expressed in terms of the
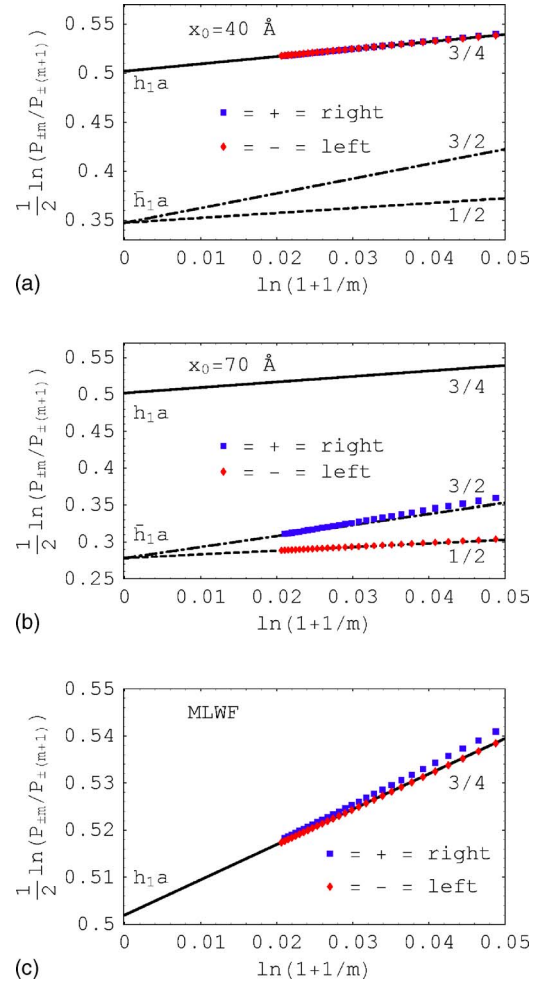

(a)

(b)

(c)

FIG. 14. (Color online) The same as Fig. 11, but for the structure SL2. Moreover, x_0 is 40 Å and 70 Å in (a) and (b), respectively.

antiderivative of the Berry connection. Then, we demonstrated that the MLWF is, except for a meaningless constant phase, a real function. This is why, when looking for the MLWF, we may limit ourselves to deal with real WFs.

Before the phase optimization the BFs were obtained by the transfer-matrix technique and the Bloch condition was applied to an initial position x_0. Following Kohn,[1] the phase of the Bloch states was fixed by imposing that either the wave function or its position derivative should be positive for all wave numbers. Therefore, two classes of WF were obtained. They are denoted as either $P\psi$WF or $P\varphi$WF. In the second stage, the phase was shifted to obtain the MLWF. Moreover, we proved that (i) the MLWF does not depend on x_0, and (ii) in a centrosymmetric crystal the MLWFs are Wannier-Kohn functions.[1–3]

Furthermore, we have analyzed the asymptotic behavior of the Wannier functions in symmetric and nonsymmetric crystals. The maximally localized Wannier functions showed isotropic exponential and power-law decays. This result has been claimed before,[5] without giving any details or proofs. Nonoptimal Wannier functions showed reduced exponential[10] and anisotropic power-law decays. This is explained by the existence of additional branch points in the

analytic continuation of the BFs to the complex wave number plane.

The theory was illustrated with numerical calculations of Wannier functions for conduction electrons in semiconductor superlattices. We already know that Wannier-Kohn functions[3] can be classified as PψWF or PφWF. Interestingly, in the considered noncentrosymmetric structure, the MLWF is a PψWF. Therefore, we wonder whether the MLWF can always be found in one of the two classes. This requires further research. If the answer were positive, the second stage, where the phase of the BFs is optimized, would be substituted by a suitable choice of the initial position. Moreover, this would help to analytically predict the asymptotic behavior of the MLWF. The extension of this formalism to generalized Wannier functions of various bands in one dimension as well as in higher dimensions is in progress.

ACKNOWLEDGMENTS

APPENDIX A: DETERMINANT OF THE TRANSFER MATRIX

The determinant of the transfer matrix $T(E;x,x_0)$ in Eq. (33) is

$$W(E,x) = \psi_{1,E}(x)\varphi_{2,E}(x) - \psi_{2,E}(x)\varphi_{1,E}(x). \quad \text{(A1)}$$

Since $\varphi_E(x) = am_e\psi_E'(x)/m^*(x)$, we note that $W(E,x)$ is $am_e/m^*(x)$ times the Wronskian of $\psi_{1,E}(x)$ and $\psi_{2,E}(x)$.

On the one hand, we note that $W(E,x)$ does not depend on x. In fact, differentiating in x on both sides of Eq. (A1), we obtain

$$\frac{\partial W}{\partial x}(E,x) = \psi_{1,E}(x)\frac{\partial \varphi_{2,E}}{\partial x}(x) - \psi_{2,E}(x)\frac{\partial \varphi_{1,E}}{\partial x}(x). \quad \text{(A2)}$$

Moreover, for a given eigenvalue E of the Hamiltonian in Eq. (29), the eigenfunctions satisfy

$$-\frac{\hbar^2}{2m_e a}\frac{\partial \varphi_E}{\partial x}(x) = [E - V(x)]\psi_E(x). \quad \text{(A3)}$$

Hence, we easily get

$$\frac{\partial W}{\partial x}(E,x) = 0. \quad \text{(A4)}$$

On the other hand, due to Eq. (31), we have $W(E,x_0)=1$. Therefore, $W(E,x)=\det[T(E,x,x_0)]=1$ for all values of E and x_0. Furthermore, since $M(E,x_0)=T(E;x_0+a,x_0)$, we also get

$$\det[M(E,x_0)] \equiv 1. \quad \text{(A5)}$$

APPENDIX B: NORMALIZATION OF BLOCH FUNCTIONS

The Bloch function $\psi_{j,k}(x)$ satisfies the Schrödinger equation $\hat{H}\psi_{j,k}(x)=E\psi_{j,k}(x)$. Here we allow k to take complex

values, but treat E as a real variable. This imposes restrictions on the values of k. If $k=k_1+ik_2$, where k_1 and k_2 are real numbers, Eq. (37) leads to

$$\cos(k_1 a)\cosh(k_2 a) - i\sin(k_1 a)\sinh(k_2 a) = \mu(E_{j,k}). \quad \text{(B1)}$$

Here, since $E_{j,k}$ is real, we have $k_2=0$ or $\sin(k_1 a)=0$. In the first case $k=k_1$ is real and we return to Eq. (37), thus obtaining the energy bands. Instead, in the second case k is complex, corresponding to the energy gaps. Moreover, we obtain

$$\cos(k_1 a) = \text{sign}[\mu(E_{j,k})] \quad \text{(B2)}$$

and

$$\cosh(k_2 a) = |\mu(E_{j,k})|. \quad \text{(B3)}$$

Regarding the derivative of $\mu(E)$, differentiation in k on both sides of Eq. (37) leads to

$$\mu'(E_{j,k})\frac{dE_{j,k}}{dk} = -a\sin(ka). \quad \text{(B4)}$$

Here, we note that $\sin(ka)=\sin(k_1 a)$ is real in the energy bands, but $\sin(ka)=i\cos(k_1 a)\sinh(k_2 a)$ in the energy gaps.

For purposes of convenience, we normalize the BFs according to

$$N_{j,k} = \int_{x_0^+}^{(x_0+a)^+} |\psi_{j,k}(x)|^2 dx = 1. \quad \text{(B5)}$$

Therefore, in the energy bands, they are normalized to unity over *any* elementary unit cell. In what follows we use the Schrödinger equation to obtain an analytic expression for $N_{j,k}$.

In agreement with Eq. (A3) we have

$$-\frac{\hbar^2}{2m_e a}\frac{\partial \varphi_{j,k}}{\partial x}(x) = [E_{j,k} - V(x)]\psi_{j,k}(x), \quad \text{(B6)}$$

where $\varphi_{j,k}(x)=am_e\psi_{j,k}'(x)/m^*(x)$. On the one hand, differentiation in the variable k and multiplication by $\psi_{j,k}^*(x)$ on both sides of Eq. (B6) lead to

$$-\frac{\hbar^2}{2m_e a}\psi_{j,k}^*(x)\frac{\partial^2 \varphi_{j,k}}{\partial k\,\partial x}(x) = [E_{j,k} - V(x)]\psi_{j,k}^*(x)\frac{\partial \psi_{j,k}}{\partial k}(x)$$

$$+ \frac{dE_{j,k}}{dk}|\psi_{j,k}(x)|^2. \quad \text{(B7)}$$

On the other hand, performing complex conjugation and multiplying by $\frac{\partial \psi_{j,k}}{\partial k}(x)$ on both sides of Eq. (B6), we get

$$-\frac{\hbar^2}{2m_e a}\frac{\partial \varphi_{j,k}^*}{\partial x}(x)\frac{\partial \psi_{j,k}}{\partial k}(x) = [E_{j,k} - V(x)]\psi_{j,k}^*(x)\frac{\partial \psi_{j,k}}{\partial k}(x). \quad \text{(B8)}$$

Combining Eqs. (B7) and (B8) we obtain

$$\frac{dE_{j,k}}{dk}|\psi_{j,k}(x)|^2 = \frac{\hbar^2}{2m_e a}\left(\frac{\partial\varphi_{j,k}^*}{\partial x}(x)\frac{\partial\psi_{j,k}}{\partial k}(x) - \psi_{j,k}^*(x)\frac{\partial^2\varphi_{j,k}}{\partial k\,\partial x}(x)\right)$$

$$= \frac{\hbar^2}{2m_e a}\frac{\partial}{\partial x}\left(\varphi_{j,k}^*(x)\frac{\partial\psi_{j,k}}{\partial k}(x) - \psi_{j,k}^*(x)\frac{\partial\varphi_{j,k}}{\partial k}(x)\right).$$

(B9)

Moreover, integration in x between x_0^+ and $(x_0+a)^+$ on both sides of this equation gives

$$\frac{dE_{j,k}}{dk}N_{j,k} = \frac{\hbar^2}{2m_e a}\left(\varphi_{j,k}^*(x)\frac{\partial\psi_{j,k}}{\partial k}(x) - \psi_{j,k}^*(x)\frac{\partial\varphi_{j,k}}{\partial k}(x)\right)\Big|_{x_0^+}^{(x_0+a)^+}.$$

(B10)

Therefore, according to Eqs. (B4) and (B5), we obtain

$$\mu'(E_{j,k})\left(\varphi_{j,k}^*(x)\frac{\partial\psi_{j,k}}{\partial k}(x) - \psi_{j,k}^*(x)\frac{\partial\varphi_{j,k}}{\partial k}(x)\right)\Big|_{x_0^+}^{(x_0+a)^+}$$

$$= -\frac{2m_e a^2}{\hbar^2}\sin(ka).$$

(B11)

Now we take Eq. (1) into account. In the energy bands k is real and we obtain

$$\mu'(E_{j,k})\text{Im}[\psi_{j,k}^*(x_0)\varphi_{j,k}(x_0^+)] = -\frac{m_e a}{\hbar^2}\sin(ka).$$

(B12)

Consequently, Eqs. (46) and (48) lead to

$$\mu'(E_{j,k})|\psi_{j,k}(x_0)|^2 = -\frac{m_e a}{\hbar^2}M_{12}(E_{j,k},x_0)$$

(B13)

and

$$\mu'(E_{j,k})|\varphi_{j,k}(x_0^+)|^2 = \frac{m_e a}{\hbar^2}M_{21}(E_{j,k},x_0),$$

(B14)

respectively. Here we note that $M_{21}(E_{j,k},x_0)$ has the sign of $\mu'(E_{j,k})$ and $M_{12}(E_{j,k},x_0)M_{21}(E_{j,k},x_0) \le 0$ in the energy bands.

In the energy gaps Eqs. (1) and (B11) lead to

$$\mu'(E_{j,k})\text{Im}\left(\psi_{j,k}^*(x_0)\frac{\partial\varphi_{j,k}}{\partial k}(x_0^+)\right) = -\frac{m_e a^2}{2\hbar^2}e^{k_2 a}\cos(k_1 a).$$

(B15)

APPENDIX C: UNIQUENESS OF THE MAXIMALLY LOCALIZED WANNIER FUNCTION

Here we discuss whether the MLWF depends on the choice of the initial position x_0. To answer this question, we consider the initial positions x_0 and x_0^0. Also, we denote the corresponding BFs as $\psi_{j,k}(x)$ and $\psi_{j,k}^0(x)$, respectively. Of course, these functions can only differ by a real phase shift $\Phi_j(k)$, i.e., $\psi_{j,k}^0(x) = \exp[i\Phi_j(k)]\psi_{j,k}(x)$. To fix ideas, we assume that $\psi_{j,k}(x_0) > 0$ for every wave number k. Moreover, we suppose that $\psi_{j,k}(x_0^0)$ does not vanish for any k. Therefore, we may choose $\Phi_j(k) = -\arg[\psi_{j,k}(x_0^0)]$. This leads $\psi_{j,k}^0(x_0^0)$
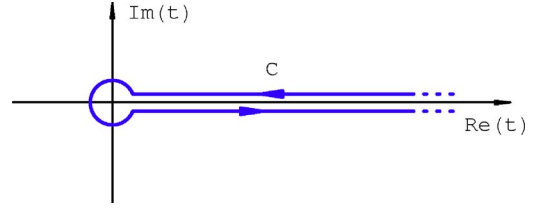

FIG. 15. (Color online) The Hankel contour in the integral representation of the gamma function.

$= |\psi_{j,k}(x_0^0)| > 0$ for every k, just as if $\psi_{j,k}^0(x)$ were produced through the first stage for x_0^0.

Now we note that $\Phi_j(k)$ is determined up to an additive constant, which is an integer multiple of 2π. However, it should be a continuously differentiable function of k. In particular, it is straightforward to show that $\Phi_j(k+2\pi/a) - \Phi_j(k) = 2R_j\pi$ and $\Phi_j(-k) + \Phi_j(k) = 2T_j\pi$, with R_j and T_j being integer numbers. Then, the relation between $\psi_{j,k}(x)$ and $\psi_{j,k}^0(x)$ is a phase shift of the type we have considered in Sec. II. In agreement with Eqs. (15) and (16), the phase shift $\Phi_j(k)$ produces the changes $X_j^0(k) = X_j(k) - \Phi_j'(k)$ and $x_j^0 = x_j - R_j a$.

Aiming the MLWF for the initial position x_0^0, which is denoted as $\tilde{w}_j^{0,ML}(x)$, we use a phase shift $\phi_j^0(k)$ with the properties $\phi_j^0(k+2\pi/a) - \phi_j^0(k) = 2r_j^0\pi$ and $\phi_j^0(-k) + \phi_j^0(k) = 2t_j^0\pi$, where r_j^0 and t_j^0 are integers. Since r_j and r_j^0 are the integer parts of $x_j/a+1/2$ and $x_j^0/a+1/2$, respectively, we have $r_j^0 = r_j - R_j$. Moreover, we take $t_j = t_j^0 = 0$ and apply Eq. (20) to obtain the phase shift leading to the MLWF as

$$\phi_j^{0,ML}(k) = r_j^0 ak + \int_0^k [X_j^0(\bar{k}) - x_j^0]d\bar{k} = \phi_j^{ML}(k) - \Phi_j(k).$$

(C1)

The corresponding BFs are

$$\tilde{\psi}_{j,k}^{0,ML}(x) = \exp[i\phi_j^{0,ML}(k)]\psi_{j,k}^0(x) = \exp[i\phi_j^{ML}(k)]\psi_{j,k}(x)$$

$$= \tilde{\psi}_{j,k}^{ML}(x).$$

(C2)

Furthermore, following Eq. (22), the MLWF is $\tilde{w}_j^{0,ML}(x) = \tilde{w}_j^{ML}(x)$. This means that the MLWF produced in the second stage does not depend on the initial position x_0.

APPENDIX D: MORE ON THE ZEROS OF $M_{12}(E,x_0)$

Let $\bar{E}$ be a root of $M_{12}(E,x_0)$, and let $\mu(\bar{E}) = \cos(\bar{k}a)$. In this case, Eq. (34) leads to

$$[e^{i\bar{k}a} - M_{11}(\bar{E},x_0)]\psi_{\bar{k}}(x_0) = 0$$

(D1)

and

$$[e^{i\bar{k}a} - M_{22}(\bar{E},x_0)]\varphi_{\bar{k}}(x_0^+) = -M_{21}(\bar{E},x_0)\psi_{\bar{k}}(x_0).$$

(D2)

Moreover, according to Eq. (A5), we have $M_{11}(\bar{E},x_0)M_{22}(\bar{E},x_0) = 1$.

If $\psi_{\bar{k}}(x_0) \ne 0$ then Eq. (D1) leads to

$$e^{i\bar{k}a} = M_{11}(\bar{E}, x_0) = \frac{1}{M_{22}(\bar{E}, x_0)}. \qquad (D3)$$

In turn, when $\psi_{\bar{k}}(x_0) = 0$ we have $\varphi_{\bar{k}}(x_0) \neq 0$. In fact, due to Eq. (32), $\psi_{\bar{k}}(x_0)$ and $\varphi_{\bar{k}}(x_0^+)$ cannot vanish simultaneously. Therefore, following Eq. (D2), we obtain

$$e^{i\bar{k}a} = M_{22}(\bar{E}, x_0) = \frac{1}{M_{11}(\bar{E}, x_0)}. \qquad (D4)$$

APPENDIX E: INTEGRAL REPRESENTATION OF THE GAMMA FUNCTION

To obtain the asymptotic behavior of the Wannier functions in Sec. VI we have used the expression[5,18]

$$\frac{1}{\Gamma(z)} = \frac{i}{2\pi} \int_C e^{-t}(-t)^{-z} dt, \qquad (E1)$$

where C is the Hankel contour depicted in Fig. 15. Note that the radius of the circle is an infinitesimal. This is an integral representation of the gamma function $\Gamma(z)$.

*Electronic address: alexys@fc.unesp.br

[1] W. Kohn, Phys. Rev. **115**, 809 (1959).

[2] F. B. Pedersen, G. T. Einevoll, and P. C. Hemmer, Phys. Rev. B **44**, 5470 (1991).

[3] A. Bruno-Alfonso and G.-Q. Hai, J. Phys.: Condens. Matter **15**, 6701 (2003).

[4] A. Bruno-Alfonso, Microelectron. J. **35**, 63 (2004).

[5] L. He and D. Vanderbilt, Phys. Rev. Lett. **86**, 5341 (2001).

[6] G. Eilenberger, Z. Phys. **180**, 43 (1964).

[7] N. Marzari and D. Vanderbilt, Phys. Rev. B **56**, 12847 (1997).

[8] V. P. Smirnov and D. E. Usvyat, Phys. Rev. B **64**, 245108 (2001).

[9] J. Bhattacharjee and U. V. Waghmare, Phys. Rev. B **71**, 045106 (2005).

[10] E. Prodan, Phys. Rev. B **73**, 035128 (2006).

[11] E. I. Blount, in *Advances in Solid State Physics*, edited by F. Seitz and D. Turnbull (Academic, New York, 1962), Vol. 13, p. 305.

[12] J. Zak, Phys. Rev. B **20**, 2228 (1979).

[13] J. Zak, Phys. Rev. Lett. **62**, 2747 (1989).

[14] J. Bhattacharjee and U. V. Waghmare, Phys. Rev. B **73**, 121102(R) (2006).

[15] M. J. Rave and W. C. Kerr, Eur. Phys. J. B **45**, 473 (2005).

[16] L. Elsgoltz, *Ecuaciones Diferenciales y Cálculo Variacional* (MIR, Moscow, 1969).

[17] This is a direct consequence of the theory presented in Sec. VI.

[18] P. M. Morse and H. Feshbach, *Methods of Theoretical Physics* (McGraw-Hill, New York, 1953), Vol. I.